AEDC-TR-91-16

C.8

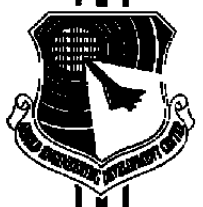

Initial Calibration of the HEAT-H2 Arc-Heated Wind Tunnel

L. M. Davis and D. B. Carver
Calspan Corporation/AEDC Operations

January 1992

Final Report for Period September 1990

ARNOLD ENGINEERING DEVELOPMENT CENTER
ARNOLD AIR FORCE BASE, TENNESSEE
AIR FORCE SYSTEMS COMMAND
UNITED STATES AIR FORCE

NOTICES

When U. S. Government drawings, specifications, or other data are used for any purpose other than a definitely related Government procurement operation, the Government thereby incurs no responsibility nor any obligation whatsoever, and the fact that the Government may have formulated, furnished, or in any way supplied the said drawings, specifications, or other data, is not to be regarded by implication or otherwise, or in any manner licensing the holder or any other person or corporation, or conveying any rights or permission to manufacture, use, or sell any patented invention that may in any way be related thereto.

Qualified users may obtain copies of this report from the Defense Technical Information Center.

References to named commercial products in this report are not to be considered in any sense as an endorsement of the product by the United States Air Force or the Government.

This report has been reviewed by the Office of Public Affairs (PA) and is releasable to the National Technical Information Service (NTIS). At NTIS, it will be available to the general public, including foreign nations.

APPROVAL STATEMENT

This report has been reviewed and approved.

BRIAN K. ANDERSON, Capt, USAF
Directorate of Aerospace Flight Dynamics Test
Deputy for Operations

Approved for publication:

FOR THE COMMANDER

EDWARD T. STRASLER
Chief, Facility Operations Division
Aerospace Flight Dynamics
Deputy for Operations

REPORT DOCUMENTATION PAGE

Form Approved
OMB No. 0704-0188

1. AGENCY USE ONLY (Leave blank)	2. REPORT DATE	3. REPORT TYPE AND DATES COVERED
	January 1992	Final - September 1990

4. TITLE AND SUBTITLE
Initial Calibration of the HEAT-H2 Arc-Heated Wind Tunnel

5. FUNDING NUMBERS
PE 65807F
PR CN66VX

6. AUTHOR(S)
Davis, L. M. and Carver, D. B.
Calspan Corporation/AEDC Operations

7. PERFORMING ORGANIZATION NAME(S) AND ADDRESS(ES)
Arnold Engineering Development Center/DOF
Air Force Systems Command
Arnold Air Force Base, TN 37389-5000

8. PERFORMING ORGANIZATION REPORT NUMBER
AEDC-TR-91-16

9. SPONSORING/MONITORING AGENCY NAMES(S) AND ADDRESS(ES)
Arnold Engineering Development Center/DOTF
Air Force Systems Command
Arnold Air Force Base, TN 37389-5000

10. SPONSORING/MONITORING AGENCY REPORT NUMBER

11. SUPPLEMENTARY NOTES
Available in Defense Technical Information Center (DTIC).

12a. DISTRIBUTION/AVAILABILITY STATEMENT
Approved for public release; distribution is unlimited.

12b. DISTRIBUTION CODE

13. ABSTRACT (Maximum 200 words)

AEDC has added an arc-heated wind tunnel to its test facility inventory that can provide a large free-jet (up to 42 in. diam at the nozzle exit) hypersonic flow. The tunnel, designated HEAT-H2, is capable of true temperature, true pressure simulations at speeds up to 15,000 ft/sec and altitudes up to 165,000 ft. Flow Mach numbers from 4 to 8 can be achieved with the existing nozzles. Included herein is a description of the test facility, along with initial calibration results obtained from one nozzle/throat combination.

The calibration was performed using a 1.5-in.-diam throat and a 24-in. exit diam, 8-deg half-angle conical nozzle. Arc heater chamber conditions ranged from 32 to 66 atm pressure, with total enthalpy from 1,560 to 2.160 Btu/lbm. Measurements within the free jet included distributions of pitot pressure, total enthalpy, and flow angle. Surface pressure distributions on a blunt cone were also obtained.

14. SUBJECT TERMS	15. NUMBER OF PAGES
calibration, hypersonic, flow field, wind tunnels, arc heater	81
	16. PRICE CODE

17. SECURITY CLASSIFICATION OF REPORT	18. SECURITY CLASSIFICATION OF THIS PAGE	19. SECURITY CLASSIFICATION OF ABSTRACT	20. LIMITATION OF ABSTRACT
UNCLASSIFIED	UNCLASSIFIED	UNCLASSIFIED	Same as Report

PREFACE

The work reported herein was performed by Calspan Corporation/AEDC Operations, operating contractor for Aerospace Flight Dynamics testing at the Arnold Engineering Development Center (AEDC), Air Force Systems Command (AFSC), Arnold Air Force Base, TN. The work was performed under Program Element 65807F and AEDC Project CN66VX. The Air Force Project Manager was Lt S. Tennent.

The HEAT-H2 arc-heated wind tunnel was initially operated in August 1989 with a successful one-run acceptance test, and the initial calibration was completed during September 1990.

The authors gratefully acknowledge Mr. R. Christenson for providing the theoretical pressure distribution solutions on the blunt cone model.

CONTENTS

ILLUSTRATIONS

Figure Page

TABLES

Table Page

APPENDIXES

1.0 INTRODUCTION

AEDC has added an arc-heated wind tunnel to its test facility inventory that can provide a large free-jet (up to 42-in.-diam) hypersonic flow. The tunnel, designated HEAT-H2 (Fig. 1), uses air for true temperature, true pressure simulations at estimated velocities up to 15,000 ft/sec and altitudes up to 165,000 ft. A calibration was performed to evaluate the test section characteristics for one nozzle configuration (1.5-in.-diam throat and a 24-in. exit diam). This document summarizes the tunnel capabilities along with the test section characteristics defined from the calibration.

Recent emphasis on the development of hypersonic vehicles makes arc-heated tunnels a natural choice for use in their development. This is particularly evident when long-duration testing is necessary. Illustrated in Fig. 2 are various types of high-temperature tunnels compared in terms of flow duration. Only arc-heated tunnels can provide temperatures equivalent to velocities greater than 10,000 ft/sec for run times of more than 1 sec.

HEAT-H2 (Fig. 1) has a high altitude simulation capability since it uses an enclosed test cell that is evacuated via a diffuser connected to a vacuum plant. The nozzle sections and diffusers were obtained from the 50-MW facility that was located at the Air Force Flight Dynamics Laboratory (Ref. 1). The estimated free-jet test envelope is shown in Fig. 3. With the present inventory of nozzles, it is possible to achieve altitudes from 80,000 to 165,000 ft at equivalent velocities up to 15,000 ft/sec. The altitude is derived from stagnation point (pitot) pressure measurements, and the velocity coincides with the total enthalpy at that pressure. Present capabilities are noted in Fig. 3 as zone 1 and zone 2, whereas the lower velocity simulations (zone 3) would require the addition of cold air to reduce the total enthalpy. A simple heater configuration change is required to go from zone 1 to zone 2. A facility modification is required to obtain the cold air needed for zone 3.

The HEAT-H2 offers a unique range of test capabilities. Particularly suited for thermal structures testing, the tunnel is large enough to accommodate flight vehicle components in addition to basic material samples for evaluations at high-altitude, hypersonic flight conditions. The tunnel is being modified to provide a scramjet combustor test capability, using the arc heater in a direct-connect mode to simulate flight velocities of 11,000 ft/sec.

2.0 APPARATUS

2.1 TEST FACILITY

The H2 test unit (Fig. 1) is an arc-heated wind tunnel located in the AEDC High Temperature Laboratory (HTL). The H2 shares utilities, power, water, air, and data

acquisition systems with the other two arc-heated test units located in the HTL, HEAT-H1 and HEAT-HR (Ref. 2). The main components of the H2 test unit include the arc heater, nozzle, test cell, model positioner system, diffuser, and air cooler. High-pressure air is injected into the arc heater where the air is heated. The air is then expanded in the nozzle to hypersonic conditions at the test section. The flow then passes through the diffuser, air cooler, isolation valves, and ducting to the AEDC Engine Test Facility (ETF) exhauster plant where it is exhausted to atmosphere.

2.1.1 Arc Heater

An N-4 Huels-type arc heater is used as the generator of the high-temperature and high-pressure test gas. The arc heater is the same heater design used in the HEAT-HR test unit which has been operational for many years. The arc heater consists of two coaxial tubular electrodes separated by a swirl chamber as shown in Fig. 4. High-pressure air is injected into the swirl chamber, heated with a direct-current arc, and vortex stabilized along the axis of the heater. The arc is further stabilized by electromagnetic coils, known as spin coils, that are located at each end of the heater. By varying the direction and distribution of the injected air, the enthalpy profile in the test section can be either a flat (symmetric) profile or a peaked (high centerline enthalpy) profile.

2.1.2 Nozzle

A three-section, water-cooled conical nozzle (Fig. 5) with an 8-deg half angle is presently available for varying the free-jet test conditions. Exit diameters of 9, 24, and 42 in. are available. These exit diameters, together with three throat diameters (1.0, 1.5, and 2.0 in.), provide a wide range of free-stream test conditions.

2.1.3 Test Cell and Model Positioner System

The H2 test cell (Fig. 6) is a cylindrical vacuum vessel 10 ft in diameter and 21 ft long. Alternate flange adapters provide for attachment of the various nozzle exit diameters. The adapter face is located 1 in. downstream of the nozzle exit. Easy access to the models is provided by a 10-ft-diam quick-opening door, which is shown open for the photograph of Fig. 6a. Windows at five locations give multiple views for recording real-time photographic data.

The H2 Model Positioner System (MPS) is a remotely operated unit that can be programmed for various inject cycles. Models are supported by water-cooled struts that are positioned by the MPS. Model water cooling can also be provided. The MPS provides rotary injection of models into the flow, and axial positioning capability over a 24-in. range. Three pre-set axial stations are available for each run. Rotary injection cycles can be pre-programmed

to control acceleration rate, maximum rotational speed, and time of model exposure. Angular rotation rates up to 60 deg/sec are possible for model weights up to 150 lb. Heavier models may be accommodated, depending upon the number of struts used and the rotation rate requirements. Axial movement is provided by servo-controlled hydraulic cylinders, whereas the rotation is powered by electric servo motors, all located outside the test cell.

For the present calibration, four struts were used to support the models/probes as shown in Fig. 6b.

2.1.4 Diffuser and Air Cooler

Two water-cooled diffusers are available to provide optimum pressure recovery for the air prior to delivery to the exhaust plant. A conical section serves as the entrance, followed by a constant diameter throat section, and a divergent section that connects to the air cooler. The smaller diffuser has a 50-in.-diam entrance and a 26.5-in. constant diameter throat section. The larger diffuser has a 75-in.-diam entrance and a 46-in. constant diameter throat section. The entire diffuser (94 ft) rests on rollers and is permitted to expand axially, being fixed to the air cooler.

The H2 air cooler consists of three tube banks of transverse water-cooled tubes. Water passing through the cooler reduces the air temperature below the exhauster plant inlet temperature limit.

2.1.5 Exhaust Ducting and ETF Exhauster Plant

The HEAT-H2 test unit is provided with exhaust pumping capability by the ETF Basic (ETF-B) and Addition (ETF-A) Exhauster Plants. The ducting that connects H2 and the ETF exhauster plants contains several valves to allow isolation between the Plenum Evacuation System (PES) plant, 16T and 16S propulsion wind tunnels, H2, and the ETF exhauster plant. Within the ETF exhauster plant system, there are two different exhaust systems. The ETF Basic (ETF-B) exhaust system consists of six centrifugal-flow exhaust compressors. The ETF Addition (ETF-A) has two axial-flow exhaust compressors. The systems are interconnected and can be staged to accommodate a wide range of mass flow rates and pressures. The exhauster plant was configured in the 1/2 T + XS configuration for all test runs, with exhaust to atmosphere occurring through the 30- and 39-in.-diam stacks. Dilution air is inbled just upstream of the exhausters to increase the air velocity and to reduce the nitric oxide (NO) and nitrogen dioxide (NO_2) concentrations before the exhaust gas exits the plant stacks. The amount of dilution air used was based on achieving a maximum of 4-percent NOx (NO + NO_2) concentration at the stacks while maintaining the duct pressure at a minimum.

2.2 TEST ARTICLES

The test articles for the calibration consisted of five probes and one model. Size is the basic distinction that separates a "probe" from a "model." Probes are small enough to be used for defining local properties, but a model is influenced by the overall flow field. Installation of the test articles was as noted in Fig. 6, with all nosetips located at the same axial position relative to the MPS. Also, the installations allowed all nosetips to pass through the free-jet centerline as the struts were rotated through the flow.

2.2.1 Transient Calorimeter and Pitot Probes

The first strut of the MPS accommodated two probes that were mounted 8 in. apart. The first two calibration runs were made with a null-point calorimeter and a pitot pressure probe mounted (Fig. 7). A coaxial surface thermocouple probe replaced the pitot pressure probe for the last two calibration runs.

Overall geometry (Fig. 7b) of the null-point calorimeter probe and coaxial surface thermocouple probe was identical: 10-deg half angle cone with a 0.25-in. radius nose. Both probes operate by the same basic principle—the sensor can be considered to be a semi-infinite solid in the time period of interest. Temperature history measurements are reduced to heat flux as a function of time, which yields heat flux versus radial position as the probe is swept through the flow. Null-point calorimeter slugs (Fig. 7c) are fabricated from copper and installed in copper probes, and the Chromel® -Constantan coaxial surface thermocouples (Fig. 7d) are installed in stainless steel probes. Null-point calorimeters are designed so that the temperature measured at a small distance below the tip surface coincides with the outside surface temperature of a solid, unaltered body (Ref. 3). The operating principle of the coaxial surface thermocouple (Refs. 4–6) is similar to that of the null-point calorimeter. The primary difference is that with the null-point calorimeter, an assumption is made that the measured temperature history is the surface temperature history, whereas with the coaxial surface thermocouple, the measurement is at the surface.

The transient pitot pressure probe body (Fig. 7b) was fabricated from copper to serve as a heat sink to protect the pressure transducer. Response time was kept small by the close proximity of the transducer to the probe tip. Measurement lag was estimated for the free-stream pitot pressure range (2.4 to 6.8 psia) measured during the calibration. It was estimated that the measurement lag error in response to a step change would be less than 1 percent after only 0.0001 sec. This yields a position lag of less than 0.01 in. for the present data.

2.2.2 Water-Cooled Flow Angularity Probe

A water-cooled flow angularity probe (Fig. 8) was designed and fabricated at AEDC to provide flow angle measurements within the free jet. Water cooling to the nosetip was necessary to ensure survival of the probe. The nosetip (Fig. 8b) was a 23-deg half angle cone fabricated from copper. Water was supplied to the nosetip at 1.5 gpm and 1,000 psi. Four surface pressure orifices were located 0.445 in. from the tip and were spaced circumferentially 90 deg apart. The flow angle relative to the probe is a direct function of the pressure difference across orifices 180 deg apart. Pressure measurements were made with four 1-psid Druck® differential pressure transducers referenced to near-vacuum. The transducers were mounted inside a protective cylinder which was not water cooled, but used silica phenolic and graphite heatshields to protect the stainless steel support hardware. The transducers were mounted on a copper heat sink that was insulated from the supporting hardware to isolate them from temperature changes. Measured heat sink temperatures varied no more than 5°F during a calibration run.

2.2.3 Water-Cooled Pitot Pressure Probe

The water-cooled pitot pressure probe (Fig. 9) used the same design concept as the flow angularity probe (see Sec. 2.2.2). The copper nosetip was cooled with water supplied at 1.5 gpm and 1,000 psi. Pressure at the tip was measured by a 15-psid Druck transducer referenced to near-vacuum. The transducer was mounted and protected in the same manner as the flow angularity probe. Both temporal and spatial measurements were possible with the probe since it could be stopped on the flow centerline, rather than swept like the transient pitot pressure probe described in Sec. 2.2.1. The effective time constant (time to 63-percent of a step change) was about 0.0013 sec at the maximum measured pressure (approximately 6.8 psia).

2.2.4 Blunt Cone Pressure Model

A 7-deg half angle blunt cone pressure model (Fig. 10) was used to evaluate the overall flow quality. The stainless steel cone model used a 0.5-in. radius copper nosetip. The copper nosetip served as a heat sink and made it possible to pause the model in the flow for a short duration. Maximum temperature at the tip never exceeded 500°F during the tests. A pressure orifice was located at the stagnation point (X = 0), and at 27 other locations along the surface in 90-deg planes around the cone surface. The stagnation point pressure was measured with a 15-psid Druck® differential pressure transducer, and the other pressures were measured with a 2.5-psid, 32-channel Electronically Scanned Pressure (ESP) module manufactured by Pressure Systems, Inc. A near-vacuum reference was used for all measurements. The transducers were mounted inside a water-cooled box, and a heater element was used to maintain the transducer temperature at 125°F ± 2°F throughout the tests.

2.3 INSTRUMENTATION

2.3.1 HTL Digital Data Acquisition System

The HTL Digital Data Acquisition System (Ref. 2) is the standard system for acquisition and recording of facility and test model data. Facility data consisted primarily of data from venturis and flowmeters used for air and water flow measurements, respectively, thermocouples used for temperature measurement, strain-gage transducers used for pressure measurement, transducers used for electrical current measurement, and dividers used for voltage measurement. Facility data are recorded in the normal- or low-speed data mode. Additionally, model data can be recorded on available low-speed data mode channels or in the high-speed mode, if required.

2.3.2 Rapid Data System

The Rapid Data System (RDS) is a portable data acquisition system consisting of a central processing unit, disk drives, terminal, printer, and an analog-to-digital converter. The RDS was installed to provide recording of the calibration model and probe data.

2.3.3 Non-Intrusive Measurements

Measurements of the NOx concentration level in the facility exhaust were obtained at the ETF exhaust stacks using a chemiluminescence system. The data were obtained as a measurement and monitor of air pollution.

A diverging beam shadowgraph system was installed in an attempt to obtain qualitative data on the flow-field structure. The system included a Class III laser as the light source mounted on top of the test cell, and a 4- by 6-ft Scotchlite® screen mounted on the floor of the test cell as the reflector. This system was not used after the second test run because the low Reynolds number per foot (approximately 100,000 to 300,000) of the flow field prevented shadow imaging with this system. Development of an improved shadowgraph system or a schlieren system that could provide the desired imaging was beyond the scope of this test.

3.0 PROCEDURE

3.1 TEST CONDITIONS

Testing was conducted with the 24-in. exit diam nozzle and 1.5-in.-diam throat. The 0.242-in.-diam arc heater air injectors were configured to provide a flat enthalpy profile. A 96-in. cathode was installed, and the front and rear electromagnetic spin coils were located

at their respective extreme forward and rearward locations. The arc heater power supply reactance was set at 0 ohms, and the 50-in. entrance diam diffuser was installed.

The calibration probe axial stations were measured from the nozzle exit plane. A nozzle mounting flange protrudes 1.0 in. into the test cell from the nozzle exit and limits the proximity of the probe tips to the nozzle exit. The probes were mounted so the distance from the nozzle exit to the tip of each model was identical. The forward, mid, and aft axial stations used for the H2 calibration (measured from the nozzle exit to the probe tip) were 2, 9, and 16 in., respectively.

Arc current and arc chamber pressure were varied from approximately 1,800 to 2,900 amp and 32 to 66 atm. A total of 27 sweeps of each probe/model was conducted. A run matrix is provided in Table 1.

3.2 TEST PROCEDURES

The probes were swept through 72 deg of rotation at varying rates. Some were paused on centerline by dividing the sweep into two 36-deg moves, which resulted in a pause on centerline of approximately 0.5 sec. Table 2 details the sweep sequences. Data from the calibration probes and model were recorded on the Rapid Data System. Facility data were recorded on the HTL Digital Data Acquisition System in the low-speed mode.

It was anticipated that the run time would be limited by the PES No. 5 Tap Changing Transformer winding temperature. The transformer, reactor, and rectifier are the main components of the arc heater power supply system. The transformer temperature limit at the time of the H2 calibration was 140°C (read on an analog gauge in the HTL control room). The test matrix for each test run was designed to maximize the number of probe and model sweeps based on the estimated transformer heating time. Each successful test run was terminated when the transformer temperature limit was reached. NOx emissions at the ETF exhaust stacks were measured for each test run.

3.3 DATA REDUCTION

3.3.1 General

Pressure measurements were reduced to engineering units based on calibrated scale factors and pretest measured offsets. Temperatures were computed from thermocouple millivolt outputs based on curve fits from standard thermocouple tables.

The chemical properties of the arc-heated, expanded test gas in the HEAT-H2 are not known at present. It is expected that the test gas will be in chemical nonequilibrium, primarily because of an estimated mole fraction of nitric oxide (NO) in the test gas of 4 to 7 percent. Some assumptions regarding the real gas effects on the ratio of specific heats and Mach number were made to reduce the flow angularity probe and blunt cone model data. These assumptions and their rationale are presented in the following sections.

3.3.2 Heater Parameters

Cold air supplied to the heater was metered by a choked venturi, from which the flow rate, WA, was computed. Power input to the heater (PWR_{IN}) was computed directly as the product of measured arc column voltage drop and the arc column current. Power losses (PWR_L) to the arc heater and nozzle cooling water were computed from the measured water flow rates and temperature increases. The bulk enthalpy (HO_B) was calculated from conservation of energy:

$$HO_B = [PWR_{IN} - PWR_L]/WA + H_V \tag{1}$$

where H_V = initial enthalpy of air at metering venturi.

3.3.3 Heat Flux

Data reduction for heat flux was performed by assuming that the measured temperature history, T(t), of the sensor can be used as the surface temperature history of a homogeneous semi-infinite solid. Validity of the assumption depends upon sensor construction, a proper match of material properties at the sensor/probe interface, and short exposure times.

The experimentally measured surface temperature history, T(t), is input to a short-form version of the numerical integration equation developed by Cook and Felderman (Ref. 7). The expression used was derived in 1974 by Don Wagner of Sverdrup Technology, Inc. and is shown as Eq. (2):

$$\dot{q}(t_n) = \frac{2(\varrho\ Cp\ K)^{1/2}}{\pi^{1/2}} \sum_{i=1}^{n} \frac{T_i - T_{i-1}}{(t_n - t_i)^{1/2} + (t_n - t_{i-1})^{1/2}} \tag{2}$$

where ϱ, Cp, and K are the density, specific heat, and thermal conductivity, respectively, of the model material. A close match of the lumped thermal parameter $(\varrho\ Cp\ K)^{1/2}$ for the sensor/probe materials is essential to avoid measurement errors. A perfect match for the null-point calorimeter was achieved by pressing the sensor into a test probe of the same material (copper).

For the coaxial sensor, Chromel® and Constantan thermal properties are closely matched, having lumped thermal properties within 1 percent of each other at room temperature. The coaxial sensor was installed in a 300-series stainless steel probe body which had a lumped thermal parameter less than 10-percent different than the Chromel® -Constantan thermo-elements.

Analysis showed that all assumptions were valid for the null-point calorimeter in its application for this test. This was not the case for the coaxial sensor. The use of the above equation yielded values of heat flux that were biased low by up to 30 percent. The small radius (0.25 in.) would have caused the heat flux to be high for a uniform heat flux, but this was offset by the distribution effect. The overall result was that the sensor temperature responded as if it were a semi-infinite solid with temperature-dependent material properties. The lumped thermal parameter for the coaxial sensor increased as much as 35 percent over the temperature range of the test (ambient to 800°F). Further analysis showed that this variable property effect could be accounted for outside the summation of Eq. (2). Thus, for the coaxial sensor, the lumped thermal property was defined as:

$$[(\varrho\ Cp\ K)^{1/2}]_n = \sum_{j=0}^{3} a_j (T_{2/3n})^j \qquad (3)$$

which is a polynomial fit of the material properties at a temperature two-thirds of the way into the time history. The coefficients, a_j, were defined by property data for Constantan (Ref. 8).

3.3.4 Water-Cooled Probe Pressures

Transducer output was reduced to pressure as described in Sec. 3.3.1. The measurements exhibited some pneumatic lag, which was expected for the sweep rates used. Only measurements outside the 16-in.-diam core were affected. The continuous sweep pressure prediction technique (Ref. 9) was used for final data reductions, thus correcting for observed pneumatic lag.

3.3.5 Flow Angles

The total flow angle with respect to the probe, AATCA, was calculated from the four measured pressures using theoretical variations for a 23-deg half angle sharp cone at small angles of attack (Ref 10). A curve-fit correlation (Appendix A) was derived from the theory for a constant specific heat ratio, $\gamma = 1.3$, and a Mach number range from 4 to 8. Specific heat ratios of $\gamma = 1.2$ to 1.4 were considered in the correlation, but it was determined by theory that the pressure differential across the cone was insensitive to the specific heat ratio

(Fig. 11). The fixed value of $\gamma = 1.3$ introduces a maximum bias error of less than 2 percent over the entire range considered. Functionally, the correlation for total angle of attack can be expressed by:

$$AATCA = GCOR \cdot MCOR\,[a1(DPSQ) + a2(DPSQ)^2],\ deg \qquad (4)$$

where:

GCOR = adjustments for $\gamma \neq 1.4$

MCOR = adjustments for Mach number $\neq 6$

a1, a2 = curve fit constants

$DPSQ = [(DP13/PAVG)^2 + (DP24/PAVG)^2]^{1/2}$

DP13 = PFA1 − PFA3; DP24 = PFA2 − PFA4

PAVG = (PFA1 + PFA2 + PFA3 + PFA4) / 4

PFA1, PFA2, PFA3, PFA4 = measured pressures of the probe, psia

Radial orientation of the flow with respect to the probe axis system was defined by:

$$PHI = Arctan\,[DP24/DP13 + 90(1 + DP13/|DP13|)],\ deg \qquad (5)$$

The flow angles with respect to the probe were transformed into a tunnel coordinate system as shown in Fig. 12. This transformation required that probe orientation and position be accounted for since the probe was being rotated as its position moved through an arc segment. ALPHA is always with respect to a radial line that passes through the probe and the nozzle centerline, with upward flow being considered as the positive direction. PSI is always perpendicular to that "radial line," with the positive direction being to the left when viewed from above and looking downstream. Thus, ALPHA is the flow divergence angle from nozzle centerline and PSI is the flow angle in the circumferential direction.

3.3.6 Blunt Cone Pressures

Each transducer measurement was recorded continuously at 30 samples per sec throughout each test run. The model was paused on centerline to permit pressure stabilization. A 15-point average of the pressures was defined after stabilization.

A special data reduction procedure was used that reduced the measurement uncertainty below what normally could be obtained. An online zero offset adjustment was applied to the measurements, which was possible because the model was initially in a large evacuated test cell just before being injected into the flow. It was therefore known that all pressures on the model should be equal while the model was outside the flow. The offset of each transducer from the average for all transducers was defined from the "outside flow data." This offset was small, generally less than the normally accepted transducer uncertainty value of 0.007 psi, but quite significant for model pressures that were as low as 0.06 psia.

3.3.7 Inferred Enthalpy

The local total enthalpy within the flow field is inferred from probe measurements of stagnation point heat flux and pitot pressure, using the assumption of laminar flow on a hemisphere and an approximation to the Fay-Riddell relationship (Ref. 11).

$$HINF = 6.882\ \dot{q}/(PPWCP/R_N)^{1/2} + H_W,\ Btu/lbm \qquad (6)$$

where $\dot{q}$ = heat flux, Btu/ft^2-sec

PPWCP = pressure from water-cooled pitot probe, atm

R_N = heat flux probe radius, in.

H_W = enthalpy of air at probe wall surface temperature, Btu/lbm

4.0 RESULTS

4.1 OPERATIONAL ENVELOPE

4.1.1 Demonstrated Operating Conditions

The demonstrated operating conditions for the 1.5-in.-diam throat and 24-in. exit diameter nozzle are shown in Fig. 13. The two primary control parameters, air mass flow rate and arc heater current, were varied from 5.2 to 9.8 lbm/sec and 1,820 to 2,900 amp, respectively, to generate data over the operational envelope shown. Arc heater chamber pressure between 32 and 66 atm, and bulk enthalpy between 1,560 and 2,160 Btu/lbm were achieved. Figures 13a–d present the demonstrated operating conditions for various parameters.

The startup and the initial setpoint were selected based on previous correlations for the HEAT-HR test unit. Figure 14 presents comparisons of HEAT-H2 test data and HEAT-HR correlations for air mass flow rate (Fig. 14a), arc heater chamber pressure (Fig. 14b), and

arc voltage (Fig. 14c). Appendix B contains the HEAT-HR correlation equations. The HR correlations averaged a 3-percent error in arc heater chamber pressure, a 4-percent error in arc heater voltage, and a 5-percent error in air mass flow when they were compared to the actual HEAT-H2 test values. These errors are similar to the errors of the actual HEAT-HR data to the correlations of 3 percent for chamber pressure, 6 percent in voltage, and 3 percent in mass flow. Additional HEAT-H2 data will be required to determine if the HEAT-HR correlations can be used in their existing form for predicting HEAT-H2 operating conditions, or if new correlations for the H2 test unit will be required.

4.1.2 Exhaust Measurements

The data from the chemiluminescence measurements at the ETF exhaust plant stacks are presented in Fig. 15. The results show that approximately 100 sec is required for the arc heater exhaust to reach the exhaust stack, and that the highest measured concentration of NOx was approximately 0.4 percent. These data are consistent with the maximum concentration of 0.44 percent measured during the peaked-profile H2 checkout run conducted in August 1989, and are well below the maximum allowable concentration of 4-percent NOx.

4.2 TEST SECTION CALIBRATION

4.2.1 Pitot Pressure Profiles

A summary of all pressure profiles obtained at XO = 2 is presented in Fig. 16a, normalized by the measured arc heater chamber pressure. These normalized profiles are repeatable and independent of the heater test condition.

Averages of all pitot pressure profiles and standard deviations are shown in Fig. 16b for each of the three axial stations. There is no perceivable expansion or compression wave emanating from the nozzle exit, but the flow continues to expand. The useful test core is at least 16 in. in diam, and within this 16-in.-diam core, the standard deviation is 1 to 2 percent. A slight asymmetry is noted, with about 7-percent higher pressure than the centerline. Included on Fig. 16b are values predicted from a one-dimensional expansion of equilibrium air with a total enthalpy of 2,000 Btu/lbm (Ref. 12). Geometric area ratios were used for the theoretical values without any consideration for the boundary layer. A profile taken from Ref. 1 is also shown, which is data from the same nozzle but with a 1.0-in.-diam throat ($A_{GEO}/A^* = 625$).

4.2.2 Flow Angle Probe Surface Pressure Profiles

The average of the four surface pressures from the flow angle probes was normalized by the arc heater chamber pressure, and the profiles were plotted. A summary of all profiles

obtained at XO = 2 is presented in Fig. 17a, and again the data show no dependence on heater test condition. The average of all profiles and their standard deviations is shown in Fig. 17b for each of the three axial stations. These profiles are quite similar to the pitot profiles, again showing a useful test core of at least 16 in. in diam and standard deviations of 1 to 2 percent.

4.2.3 Flow Angularity Profiles

Typical flow divergence, ALPHA, and flow circulation, PSI, angles for two axial stations are presented in Fig. 18. Included in Fig. 18a are theoretical lines for conical (or source) flow. The flow divergence data of Fig. 18a are replotted as deviations from conical theory in Fig. 18b. Maximum offset from theory is about 0.3 deg within the 16-in.-diam test core. These are "repeat" data sets, and the profiles do repeat, having similar small deviations for the same radial position.

A summary of all profiles obtained is presented in Figs. 19–20. The profiles are repeatable and independent of heater test conditions. The maximum offset of the average ALPHA profile from theory (Fig. 19) is 0.2 deg within a 16-in.-diam test core. The average PSI profile (Fig. 20) has a maximum offset of only 0.1 deg. Standard deviations of the average profiles are about 0.1 and 0.05 deg, respectively, for ALPHA and PSI within the test core. The same trends were exhibited for profiles obtained at XO = 9 and 16 in.

4.2.4 Blunt Cone Surface Pressure Data

Surface pressure distributions along the 7-deg blunt cone are presented in Fig. 21. Figure 21a shows data at all circumferential locations and repeatability for two data sets. Data at XO = 2 in. are compared with theory in Fig. 21b, and the trend is definitely that of conical (or source) flow, with a magnitude corresponding to approximately $\gamma = 1.31$. Note that the data of Fig. 21b were obtained at three different test conditions, and the repeatability is generally better than ± 2 percent.

There is a slight dependence on axial station as shown in Fig. 21c, consistent for each test condition (only one condition shown in the figure). This dependency is predicted by conical flow theory.

The theoretical distributions were calculated using a time-dependent flow-field simulation program (PARC Code, Ref. 13). The PARC Code can be used for two-dimensional, axisymmetric, or fully three-dimensional internal and external flow-field geometries. Both inviscid (Euler) and viscous (Navier-Stokes) flow-field calculations can be performed with this code. For the present case, inviscid solutions were obtained using constant specific heat

ratios and a starting line was computed from one-dimensional inviscid theory for source flow. For a source flow with constant specific heats assumed, the Mach number is only a function of radial distance from the source. Thus, the expression for Mach number, M, is related to the radial distance, R, by:

$$\left(\frac{R}{R^*}\right)^2 = \frac{1}{M}\left[\frac{(\gamma + 1)/(\gamma - 1) - 1 + M^2}{(\gamma + 1)/(\gamma - 1)}\right]^{\frac{\gamma + 1}{2(\gamma - 1)}} \tag{7}$$

where R^* = radial distance to the sonic point, and γ = ratio of specific heats.

For the present case, with a 1.5-in.-diam throat and a 24-in. diam exit, $R_E/R^* = 16$, which gives an exit Mach number of 6.19. A value of $\gamma = 1.25$ was used, together with the nozzle geometry, to define the Mach number along the starting line.

4.2.5 Temporal Pitot Pressure

The water-cooled pitot probe was paused on the nozzle centerline while the data were being recorded continuously. A 6-percent variation about the mean was observed for all data. A typical pressure-time trace is shown in Fig. 22a, and an autospectrum of the data is shown in Fig. 22b. The autospectrum does not show any predominant frequencies, but rather shows a general decay with increasing frequencies. Pneumatic time lag has a strong influence on the data, with attenuation of amplitude and phase-shift, as shown in Fig. 22c.

4.2.6 Heat Flux and Inferred Enthalpy Profiles

Heat flux was the basic measurement but total enthalpy was the desired parameter. Typical heat flux profile repeatability is shown in Fig. 23a, consisting of two probe sweeps at the same test condition with two probes (null-point calorimeter and coaxial surface thermocouple). The inferred enthalpy profiles (defined from these heat flux profiles and the pitot pressure profiles) are presented in Fig. 23b. These are profiles with the heater configured in the flat enthalpy mode. Within the 16-in.-diam core, the local average of these four data sets varies by about ± 5 percent. The average enthalpy profile within the core is reasonably symmetric with a centerline value about 14-percent higher than the edge value. The enthalpy profiles are independent of axial station as shown in Fig. 24.

All the enthalpy profile data from each test condition were averaged and normalized by the respective heater bulk enthalpy (HO_B). The result is shown in Fig. 25. Within the 16-in.-diam core, the average inferred enthalpy is about 1.4 times the heater bulk enthalpy, with a standard deviation of 5 percent.

4.2.7 Mach Number

Although the chemical properties of the HEAT-H2 flow field and the ratio of specific heats (γ) of the test gas have not yet been quantified, an initial assessment of Mach number can be made based on the flow angle probe and blunt cone model data. Since the flow field exhibits the characteristics of conical source flow as demonstrated in Secs. 4.2.3 and 4.2.4, it can be assumed that the flow angle is "known" at any point in the 16-in.-diam test core. The "known" flow angle and the measured value of DPSQ from the flow angle probe data make it possible to calculate a Mach number from the theory for sharp cones at angles of attack (Ref. 10 and Fig. 11). This technique requires an assumption of the value for γ; however, as seen from Fig. 11, DPSQ is relatively insensitive to γ. This methodology provides a nominal Mach number of 6.1 at a γ of 1.3. There is a high degree of uncertainty in this technique, on the order of $\pm$ 0.3 Mach number, primarily because of the sensitivity of the measurements. Follow-on calibration efforts should include tests to resolve the unknown properties of the flow field: chemistry, density, and velocity, among others.

5.0 CONCLUDING REMARKS

1. The HEAT-H2 was calibrated over a range of test conditions using a 1.5-in.-diam throat and 24-in. exit diam conical nozzle. A 96-in. cathode was used, and the arc heater was configured to produce a "flat" enthalpy profile. Demonstrated arc heater chamber conditions ranged from 32 to 66 atm, with total bulk enthalpies of 1,560 to 2,160 Btu/lbm.

2. A useful test core of 16 in. diam was demonstrated based on profiles of pitot pressure, flow angle, and total inferred enthalpy.

3. All measurements correlate with theory for a conical-type nozzle (source flow).

4. Flow angle variation within the test core is less than $\pm$ 0.3 deg when it is compared to conical flow theory.

5. Local inferred enthalpy profiles are repeatable and correlate with heater bulk enthalpy. The core enthalpy is nominally 1.4 times the heater bulk enthalpy.

6. Mach number in the test core is 6.1 $\pm$ 0.3 based on conical source flow theory and a γ of 1.3.

7. Further testing must be conducted to define the properties of the HEAT-H2 flow field, especially in the areas of chemical properties, density, and velocity before more definitive values of Mach number can be determined.

REFERENCES

1. Folck, J. L. and Smith, R. T. "Calibration of the AFFDL 50 Megawatt Arc Heated Hypersonic Wind Tunnel With a Two-Foot Nozzle." AFFDL-TR-69-36, August 1969.

2. *Test Facilities Handbook* (Twelfth Edition). Arnold Engineering Development Center, March 1984.

3. "Standard Method for Measuring Extreme Heat-Transfer Rates from High-Energy Environments Using a Transient, Null-Point Calorimeter." ASTM E-598-77, 1977 (Reapproved 1985).

4. Hedlund, E. R., Hill, J. A. F., Ragsdale, W. C., and Voisnet, R. L. P. "Heat Transfer Testing in the NSWC Hypervelocity Wind Tunnel Utilizing Co-Axial Surface Thermocouples." NSWC MP 80-151, March 1980.

5. Kidd, C. T. "Recent Developments in High Heat Flux Measurement Techniques at the AEDC." Proceedings of the 36th International Instrumentation Symposium, ISA Paper 90-156, May 1990, pp. 477–492.

6. Kidd, C. T. "Coaxial Surface Thermocouples: Analytical and Experimental Considerations for Aerothermal Heat-Flux Measurement." Proceedings of the 36th International Instrumentation Symposium, ISA Paper 90-126, May 1990, pp. 203–212.

7. Cook, W. J. and Felderman, E. J. "Reduction of Data From Thin-Film Heat-Transfer Gages: A Concise Numerical Technique." *AIAA Journal*, Vol. 4, No. 3, March 1966.

8. Touloukian, Y. S., et al. *Thermophysical Properties of Matter*. Vols. 1, 4, 10, and 12 (The TPRC Data Series), IFI/PLENUM, New York, 1970–1975.

9. Carver, D. B., Ward, W. H., and Byers, M. T. "Continuous Sweep Pressure Prediction Technique." AIAA Paper 86-0767, AIAA 14th Aerodynamic Testing Conference, West Palm Beach, FL, March 5–7, 1986.

10. Jones, D. J. "Numerical Solutions of the Flow-Field for Conical Bodies in a Supersonic Stream." National Research Council of Canada, Aeronautical Report LR-507, July 1968.

11. Fay, J. A. and Riddell, F. R. "Theory of Stagnation Point Heat Transfer in Dissociated Air." *Journal of the Aerospace Sciences*, Vol. 25, No. 73, February 1958.

12. Jorgensen, L. H. and Baum, G. M. "Charts for Equilibrium Flow Properties of Air in Hypervelocity Nozzles." NASA TN D-1333, September 1962.

13. Cooper, G. K. and Sirbaugh, J. R. "PARC Distinction: A Practical Flow Simulator." AIAA-90-2002, June 1990.

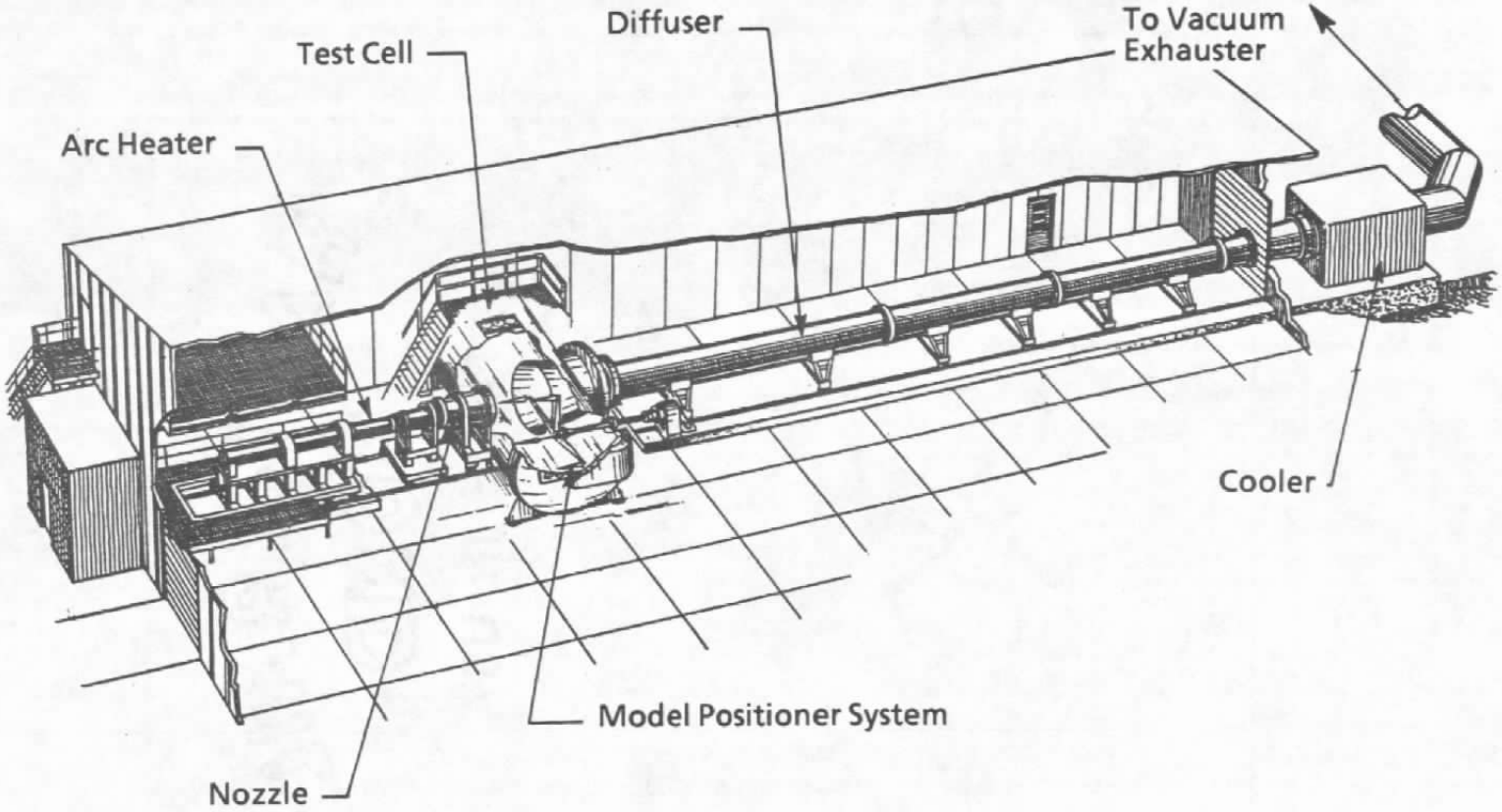

Figure 1. HEAT-H2 arc-heated wind tunnel.

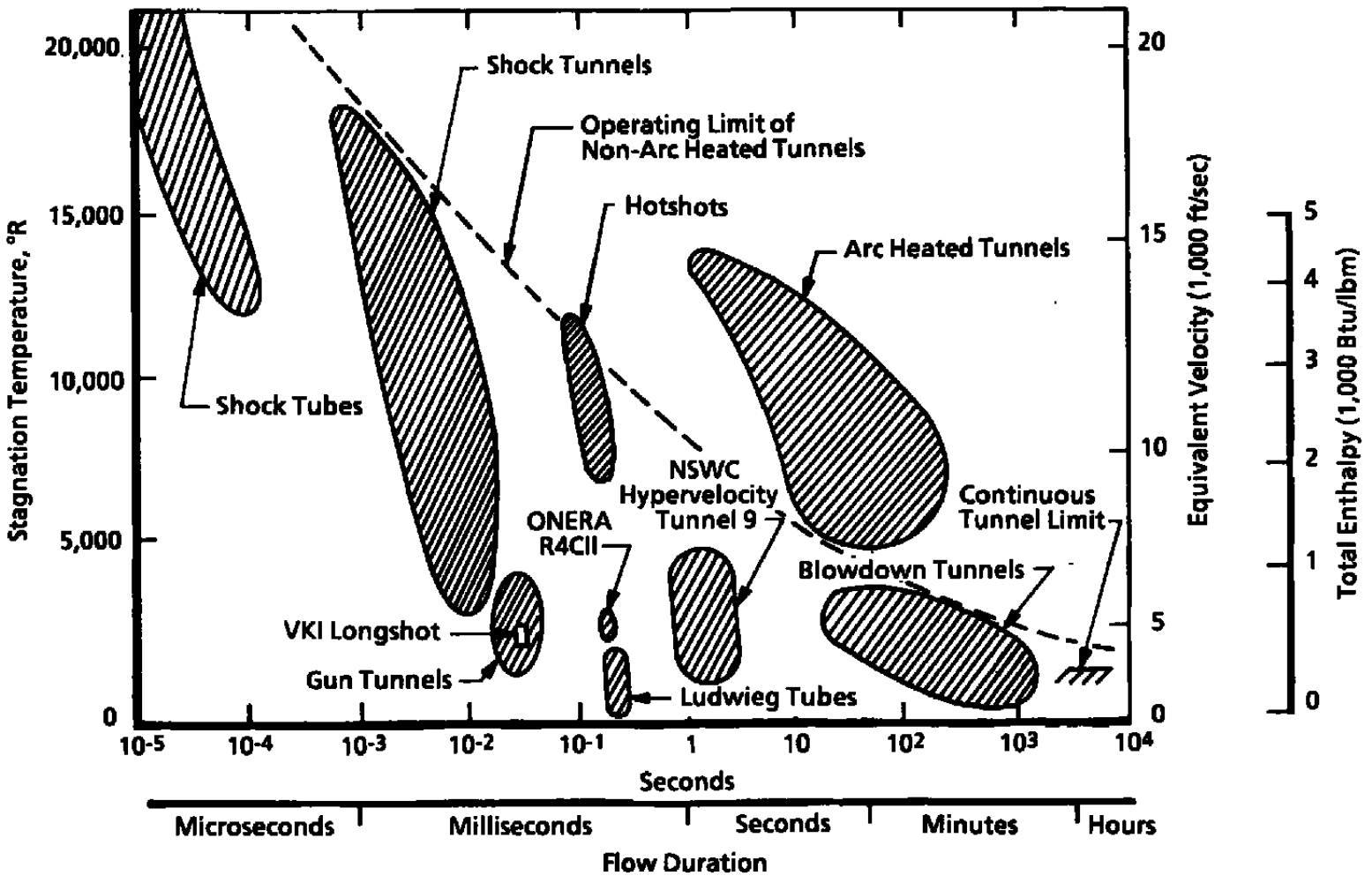

Figure 2. High-temperature tunnel capabilities.

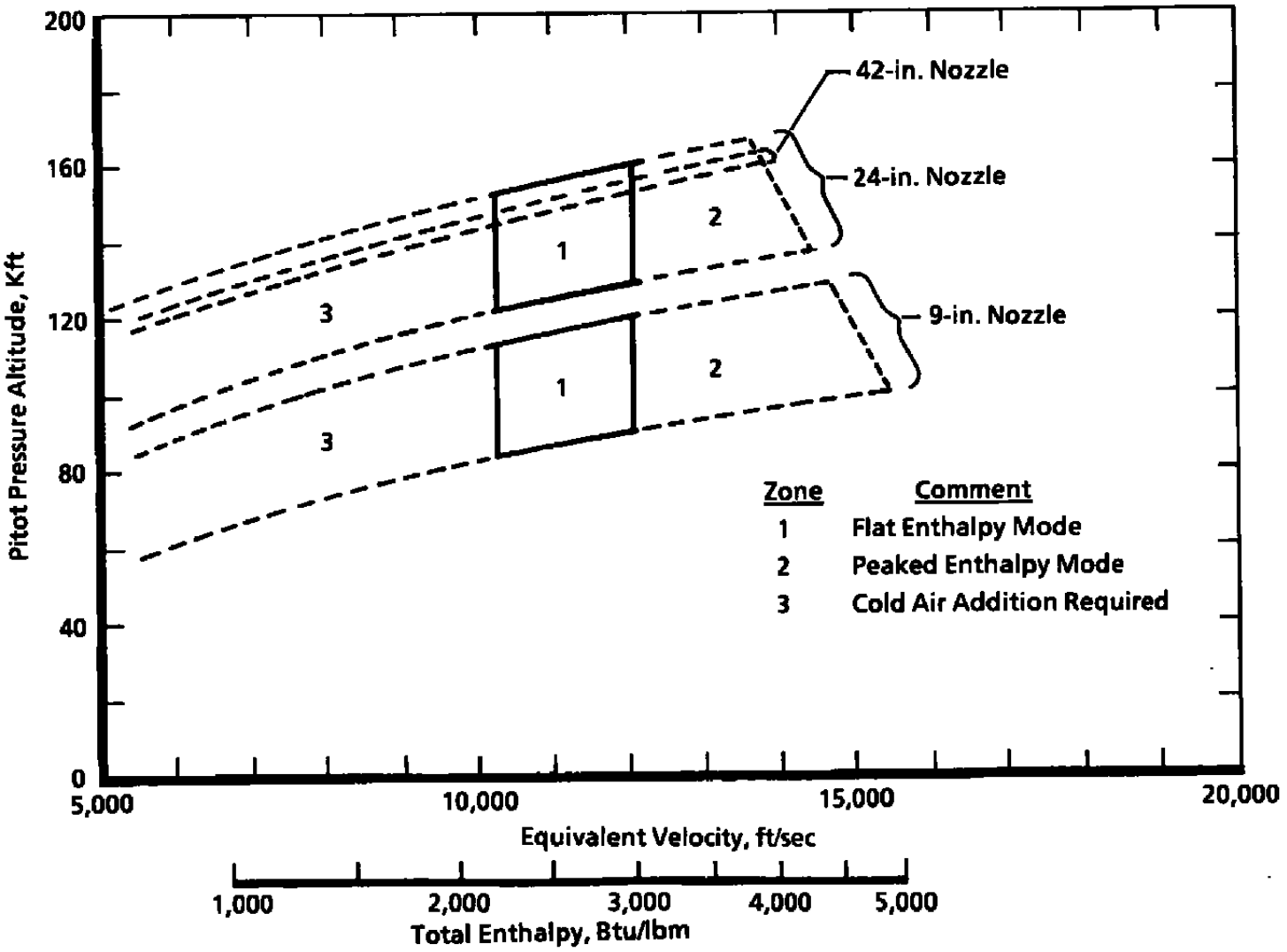

Figure 3. Estimated HEAT-H2 free-jet test envelope.

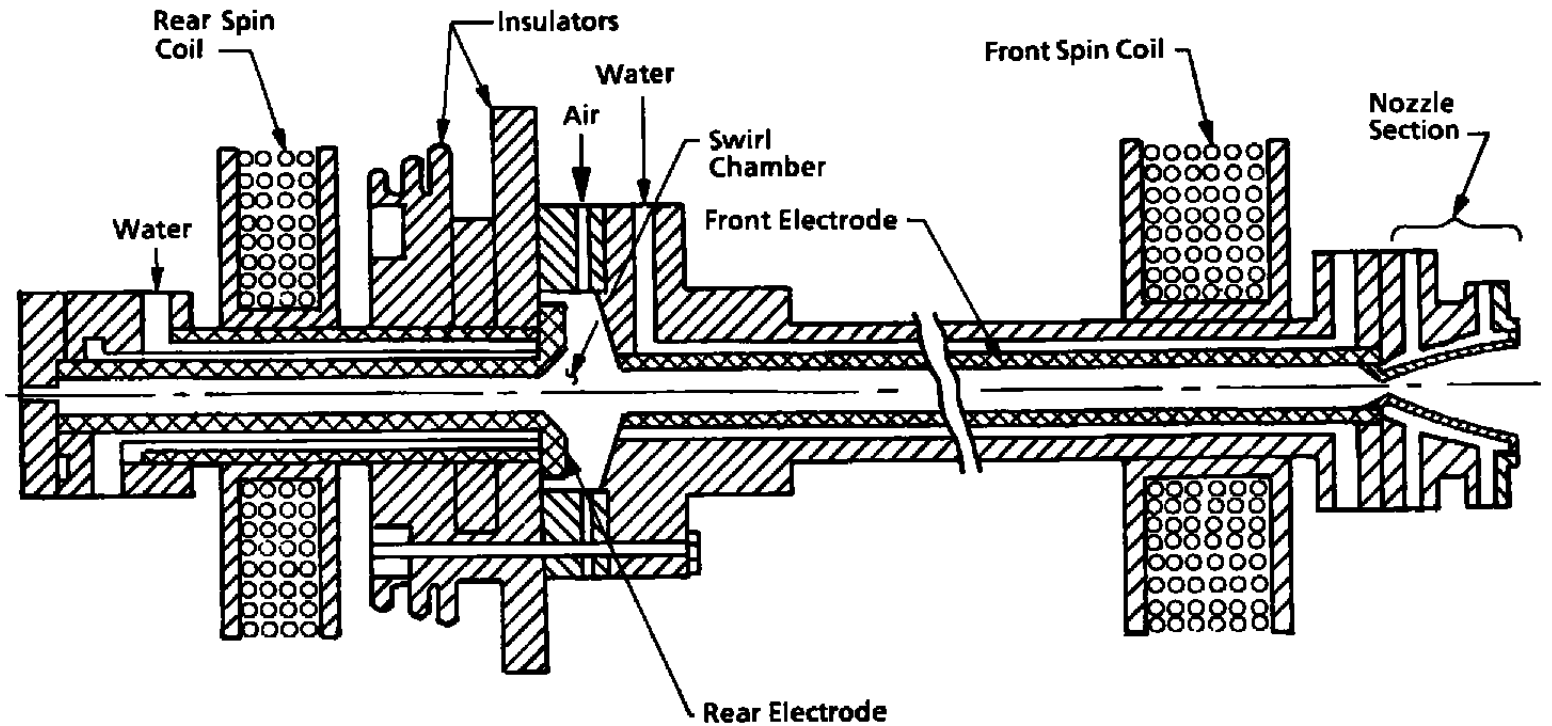

Figure 4. N-4 Huels-type arc heater schematic.

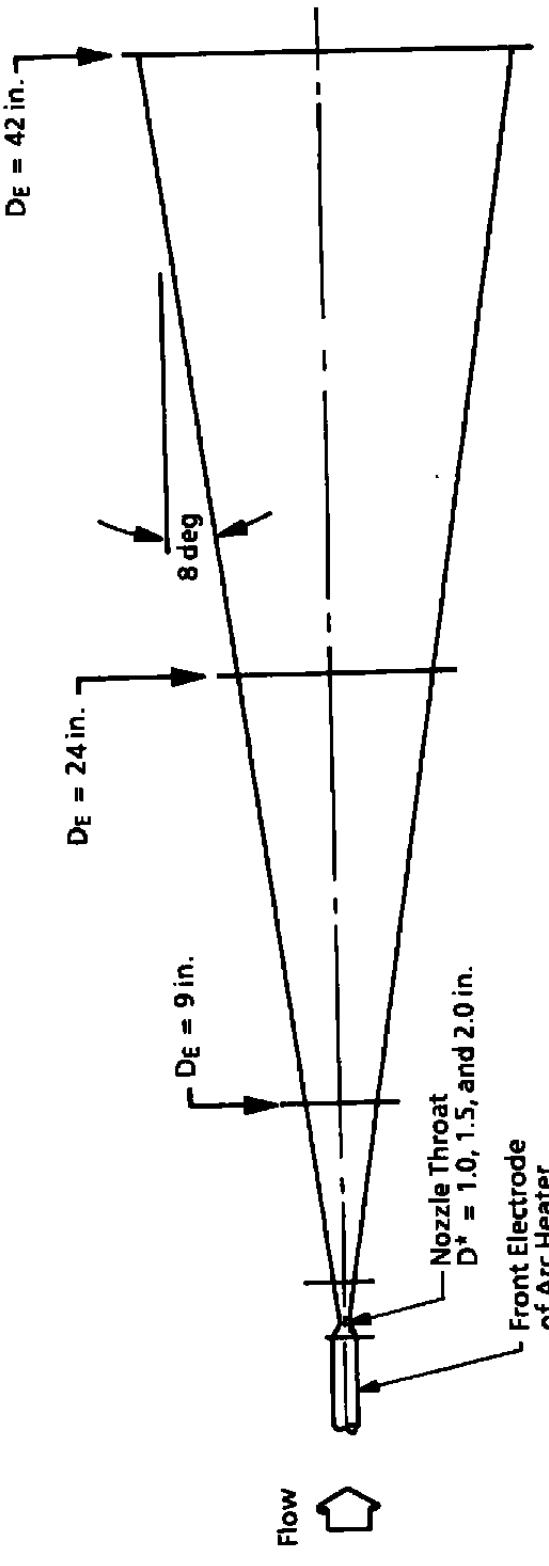

Figure 5. HEAT-H2 conical nozzle.

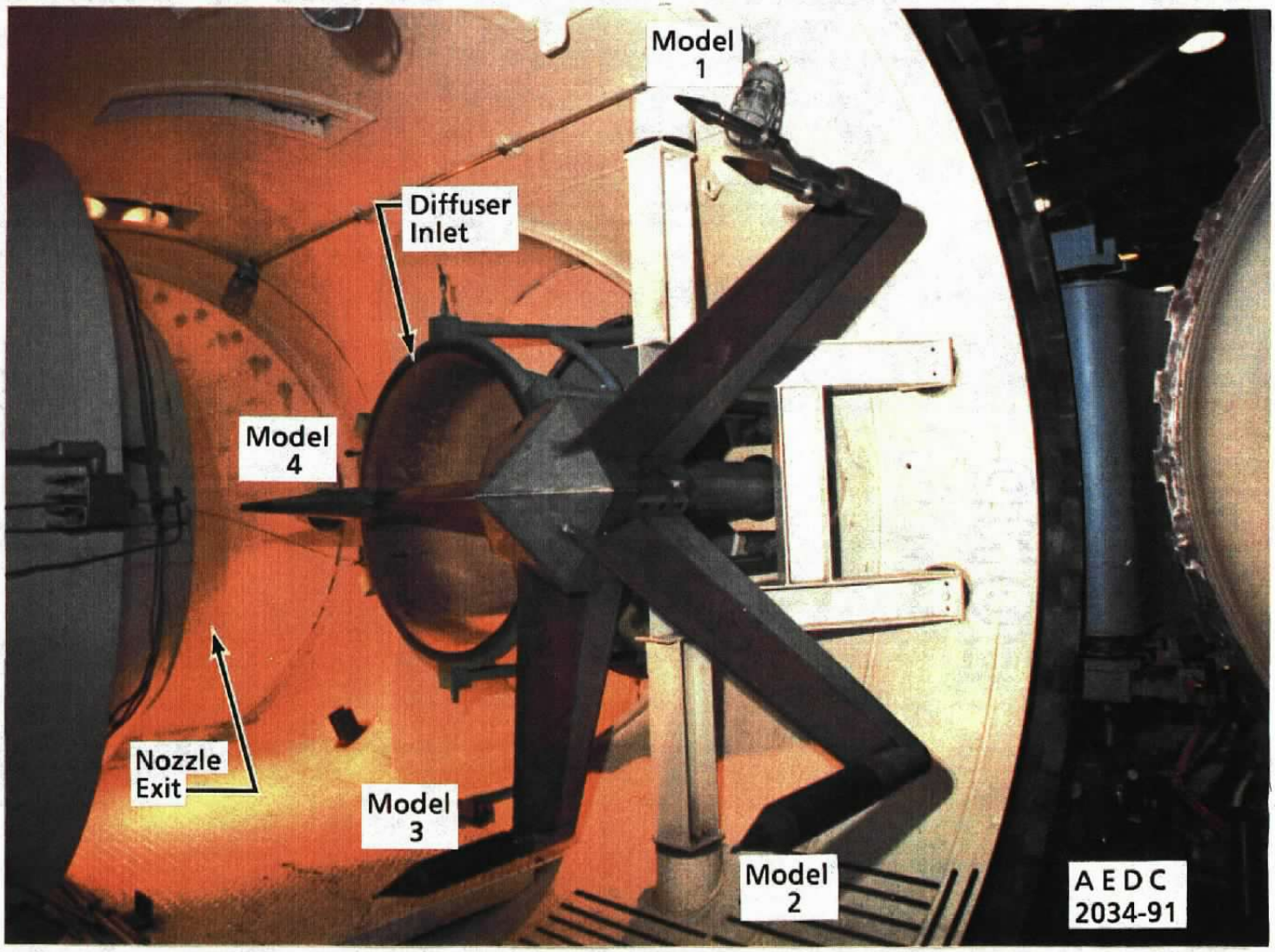

a. Photograph

Figure 6. HEAT-H2 test cell and model positioner system.

Model	Description
4	7-deg Half Angle Pressure Cone
3	Water-Cooled Pitot Pressure Probe
2	Flow Angularity Probe

Model	Description
1	Standard Null Point Calorimeter/Pitot Pressure Probes (Runs 1 and 2). Standard Null Point Calorimeter/Coax Calorimeter (Runs 5 and 6).

Note: All Dimensions in Inches

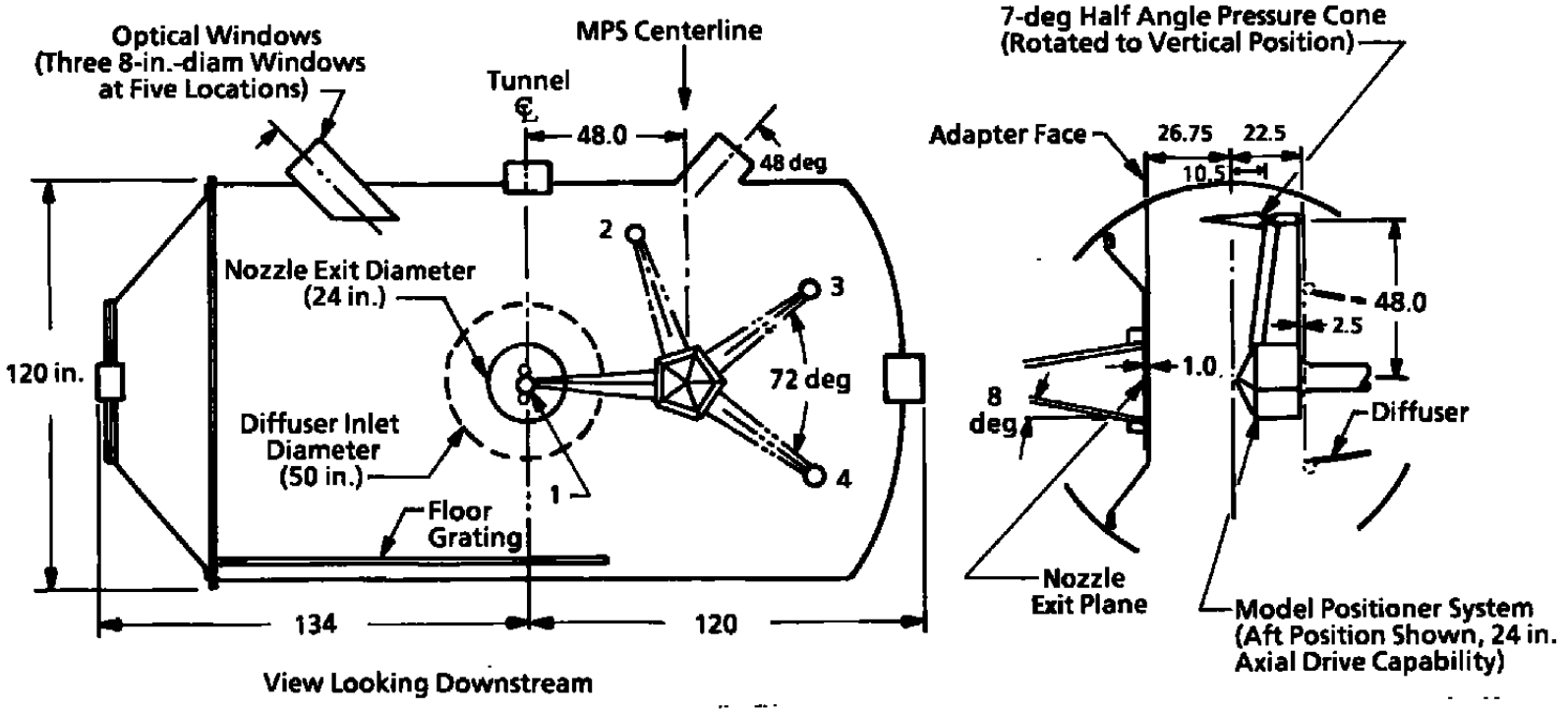

b. Details of cell and installation

Figure 6. Concluded.

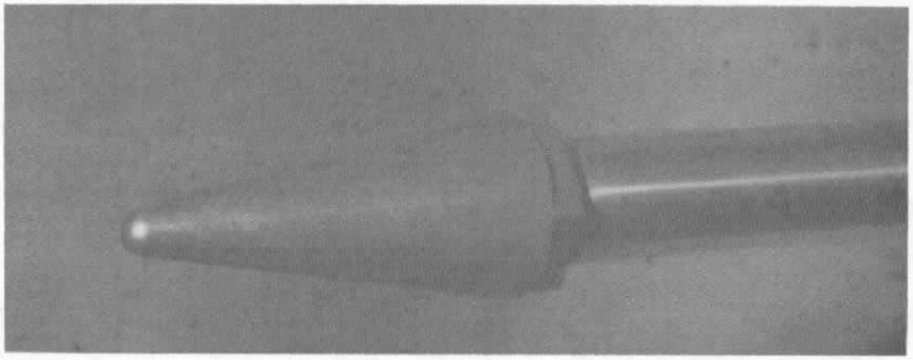

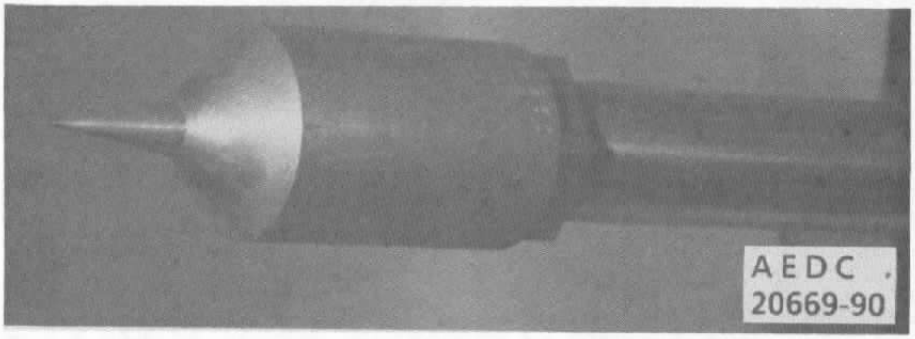

a. Photographs

Figure 7. Transient calorimeter and pitot pressure probes.

Note: All linear dimensions in inches
1. Coax gage calorimeter probe consists of a Chromel®-Constantan coaxial surface thermocouple, 1/16 in. diam, installed in the nosetip of a 304 stainless steel probe body with the same geometry as the null point calorimeter probe
2. Ref. AEDC dwgs VX113271 & VX213271
3. Shown as side view with H2 strut on nozzle centerline

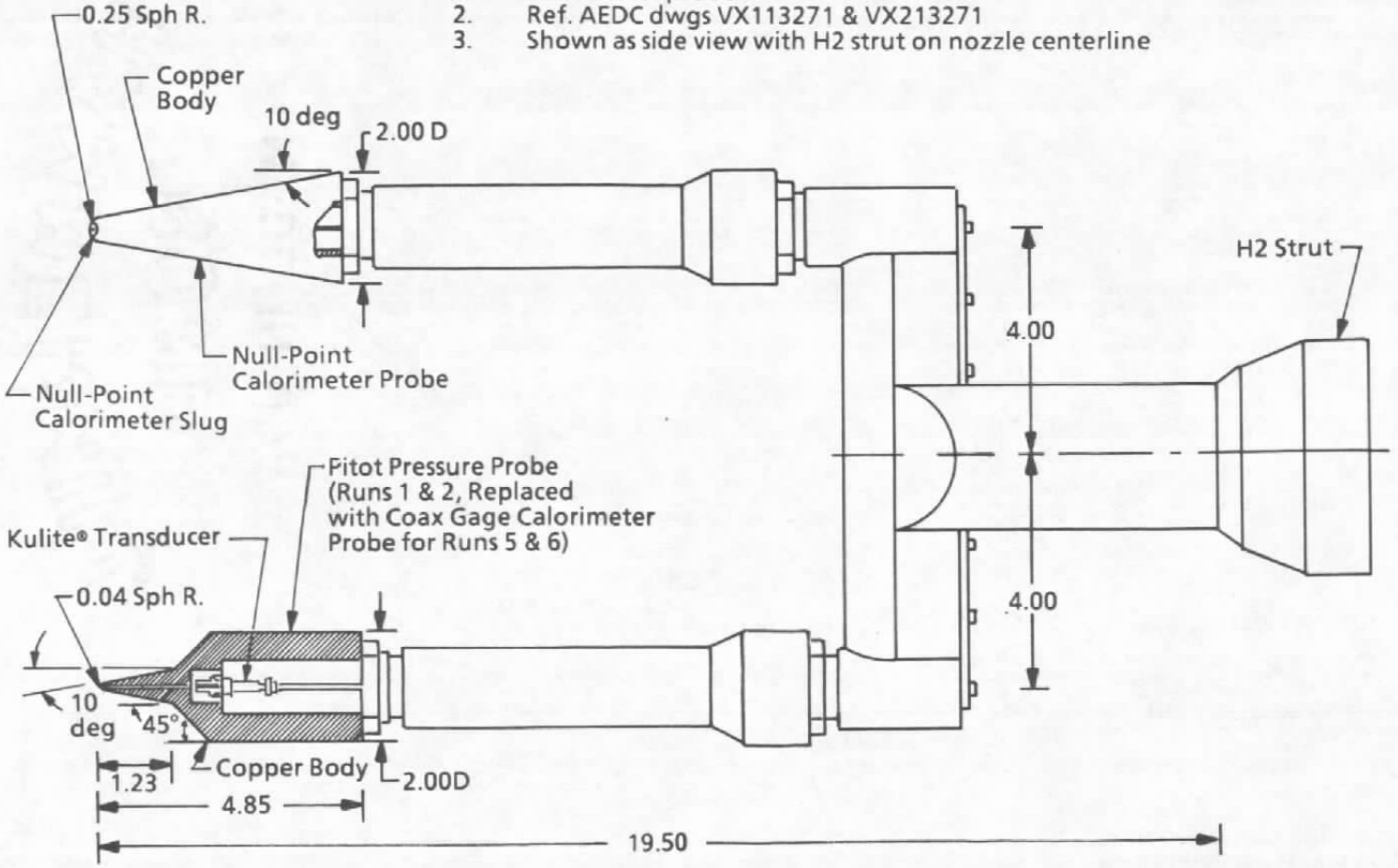

b. Details of probes and the installation

Figure 7. Continued.

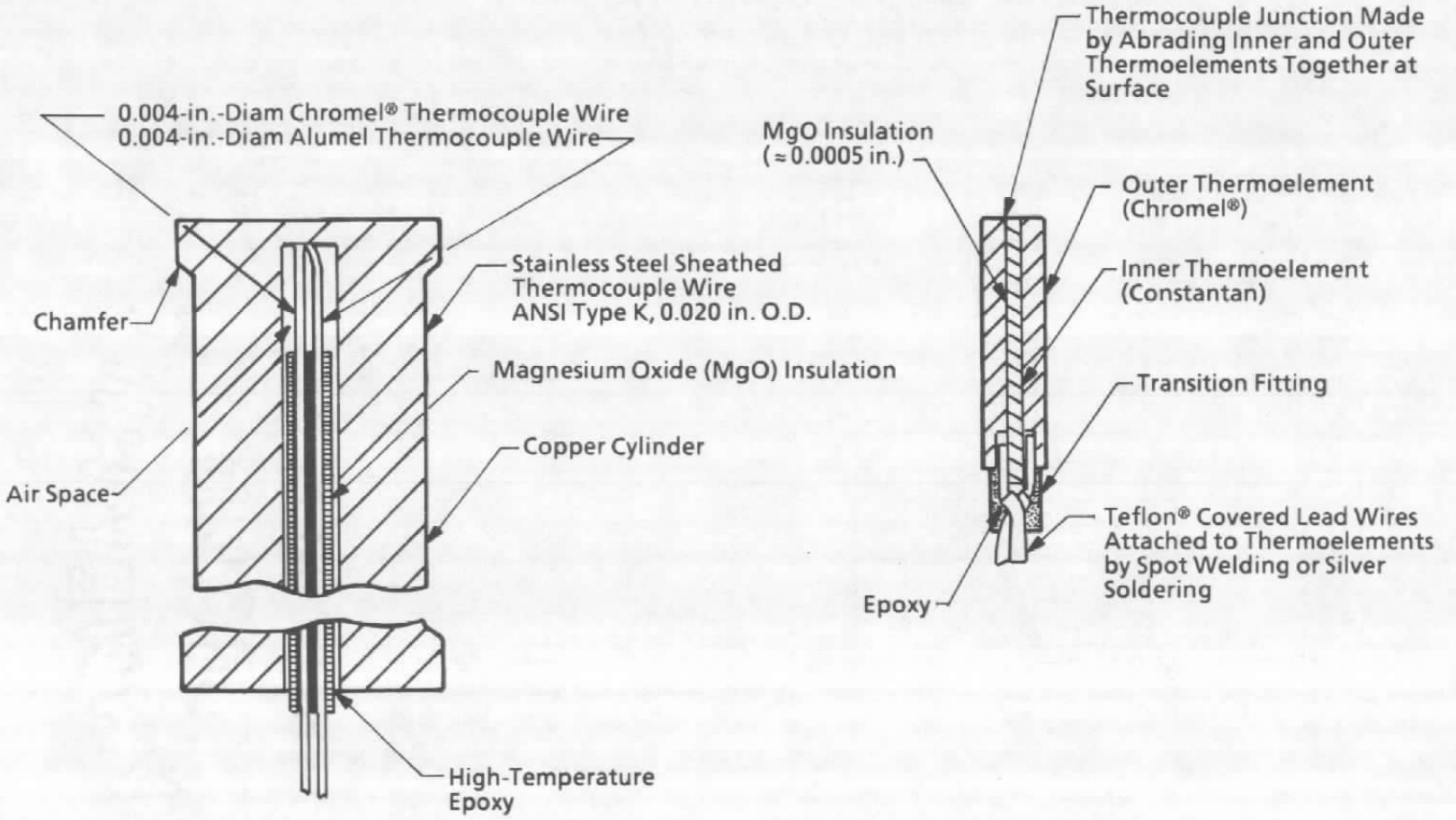

c. Section view of null-point calorimeter assembly, no scale

d. Section view of coaxial surface thermocouple, no scale

Figure 7. Concluded.

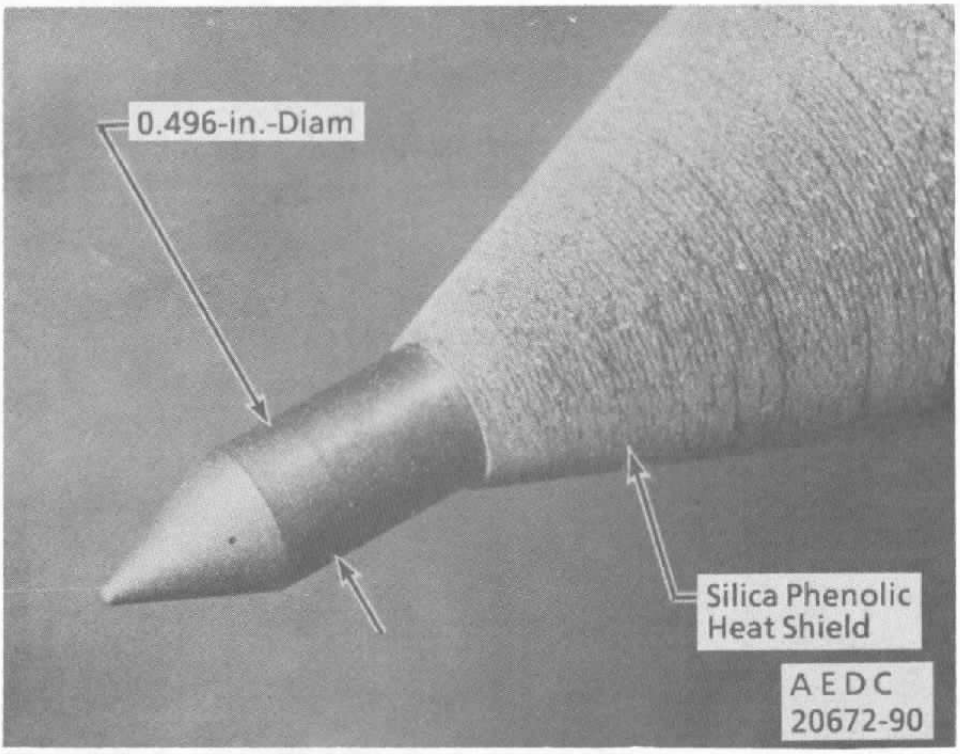

a. Photograph of probe tip

Figure 8. Water-cooled flow angularity probe.

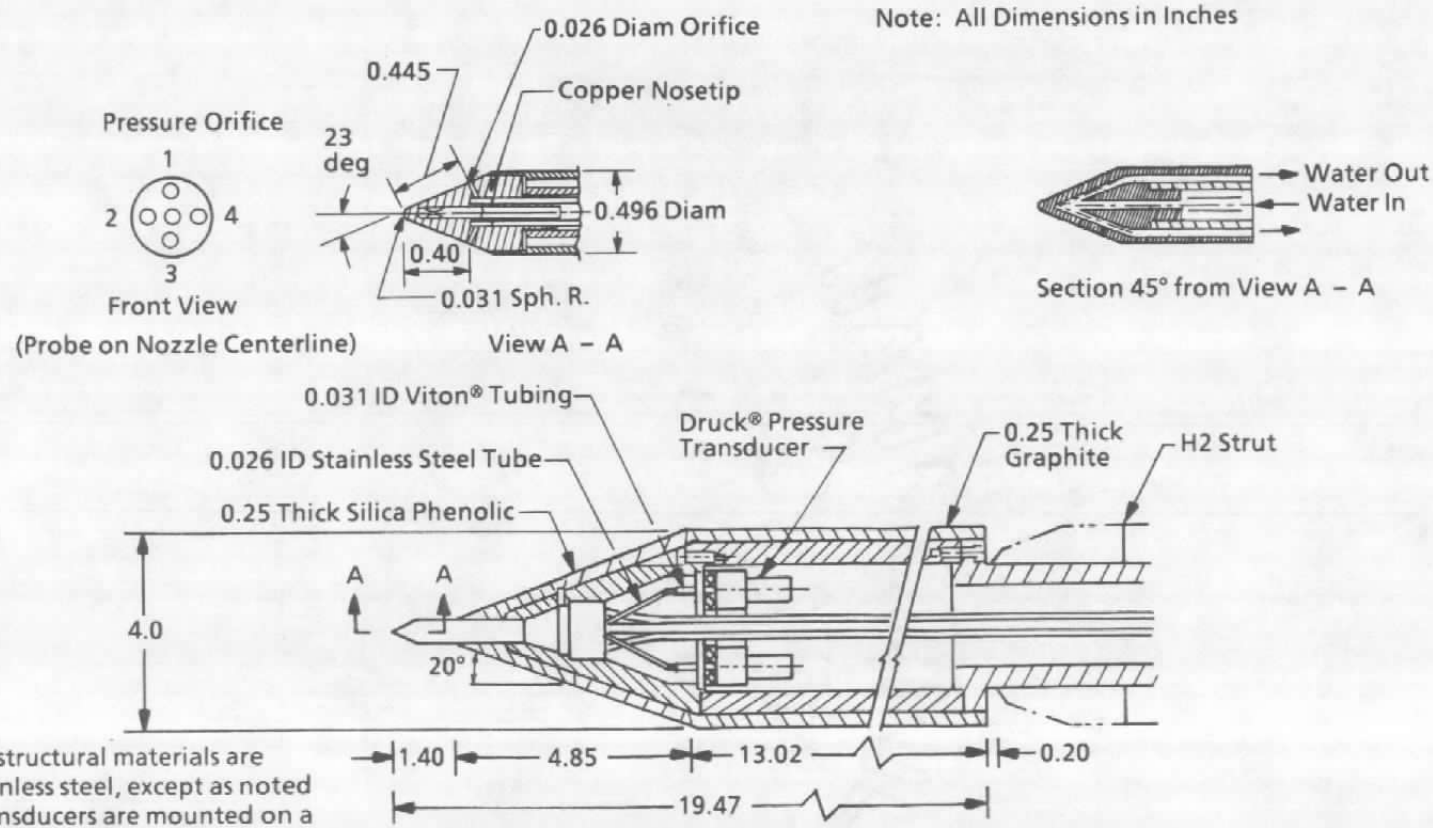

1. All structural materials are stainless steel, except as noted
2. Transducers are mounted on a 1/8-in.-thick copper heat sink, with a 3/16-in.-thick phenolic plate for thermal insulation from probe body
3. Ref. AEDC Dwg. VX21377.30

b. Details

Figure 8. Concluded.

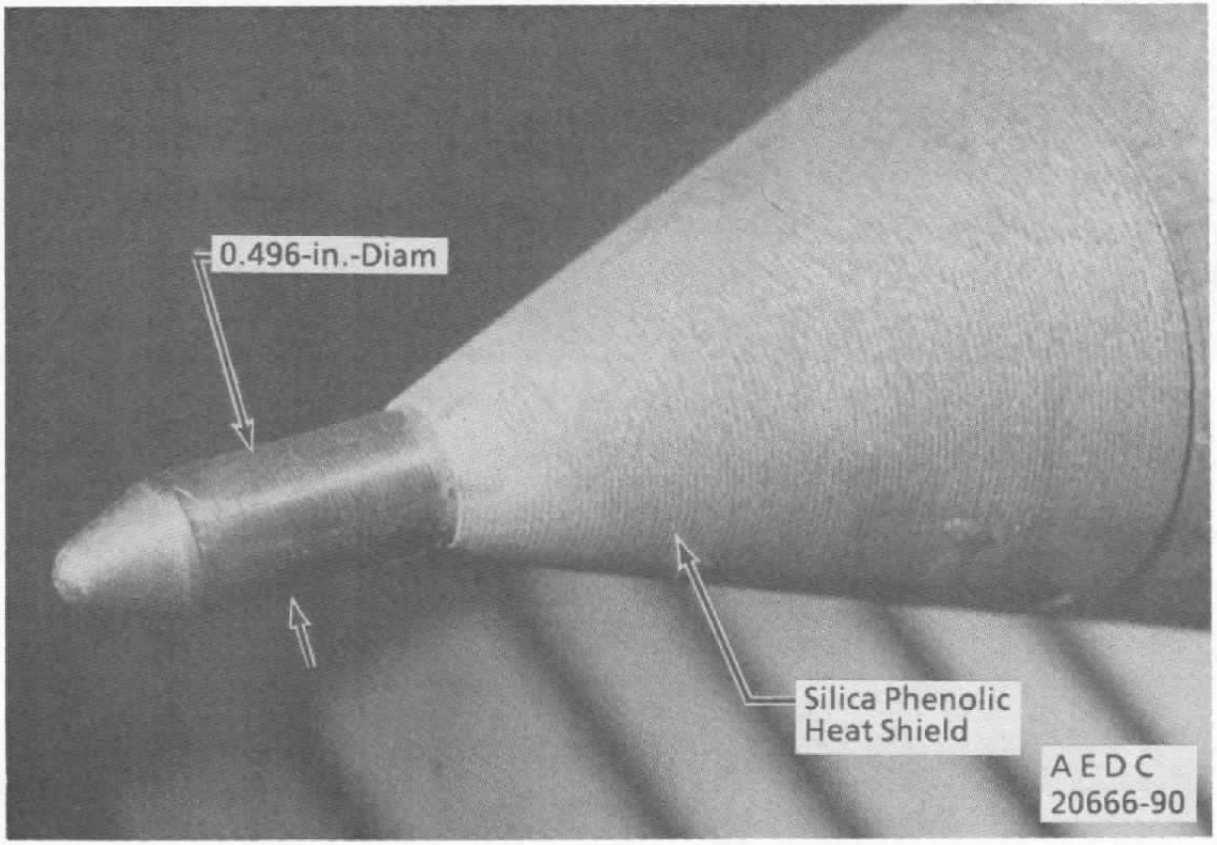

a. Photograph of probe tip

Figure 9. Water-cooled pitot pressure probe.

Note: All Linear Dimensions in Inches

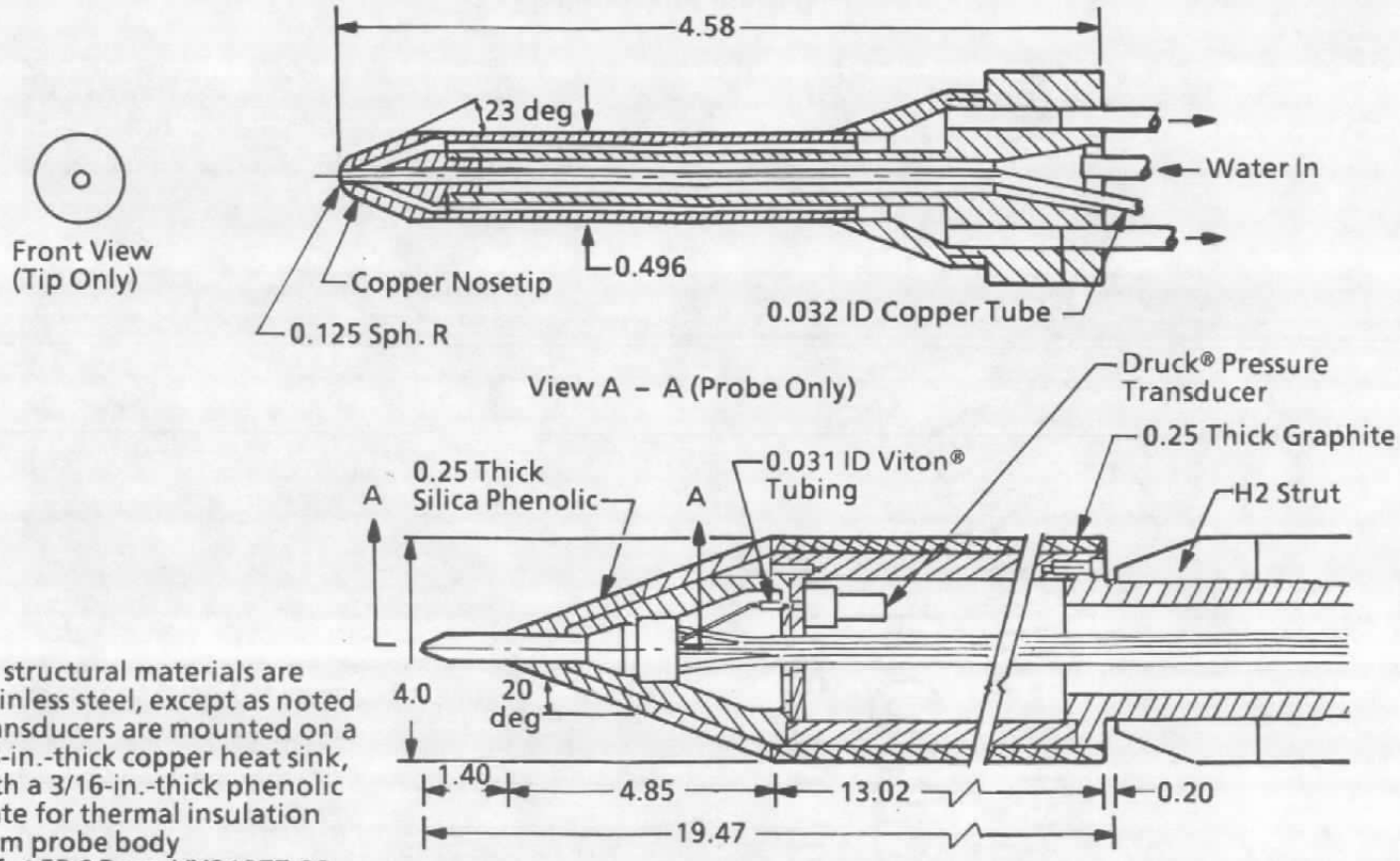

1. All structural materials are stainless steel, except as noted
2. Transducers are mounted on a 1/8-in.-thick copper heat sink, with a 3/16-in.-thick phenolic plate for thermal insulation from probe body
3. Ref. AEDC Dwg. VX21377.30

b. Details

Figure 9. Concluded.

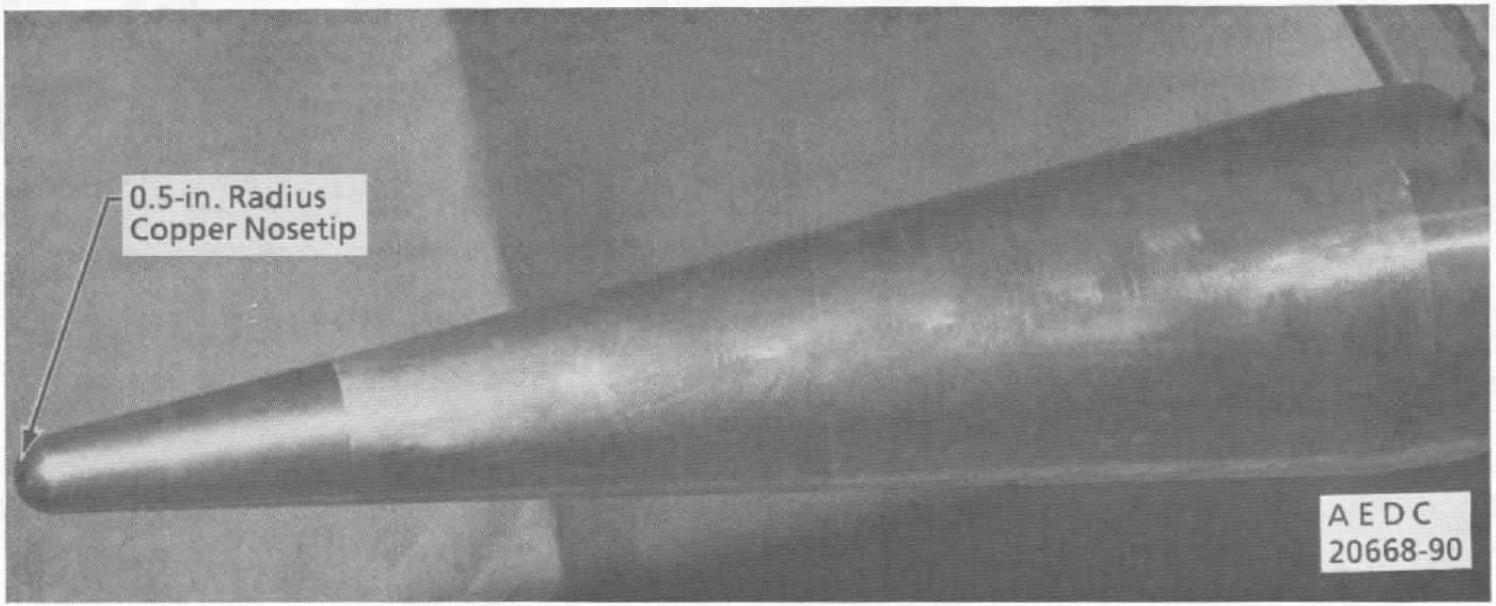

a. Photograph

Figure 10. Blunt cone pressure model.

Note: All Dimensions in Inches

1. All structural materials are stainless steel, except as noted
2. Shown as top view when model is on nozzle centerline
3. Ref. AEDC Dwg. VX213771.10

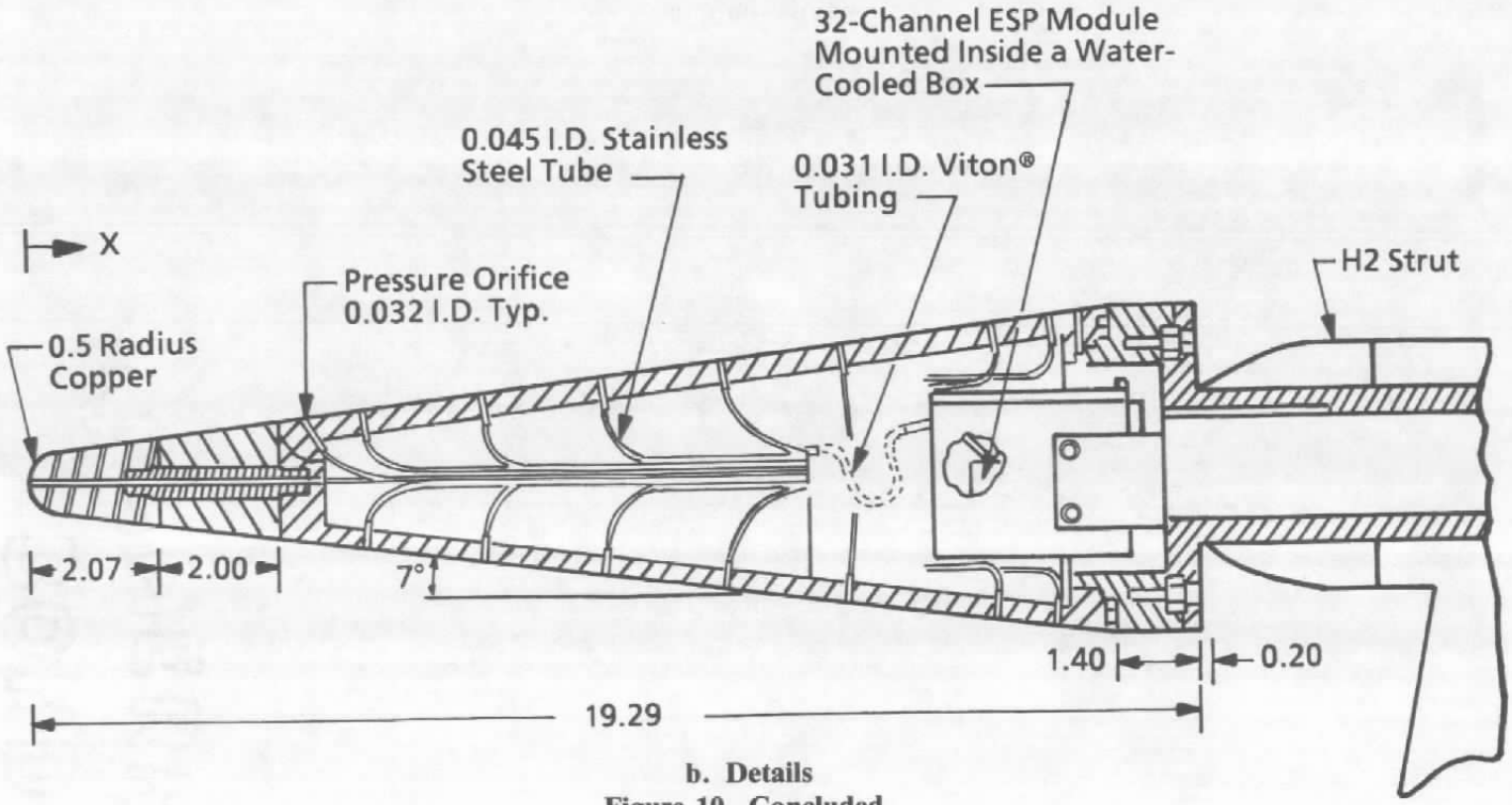

b. Details

Figure 10. Concluded.

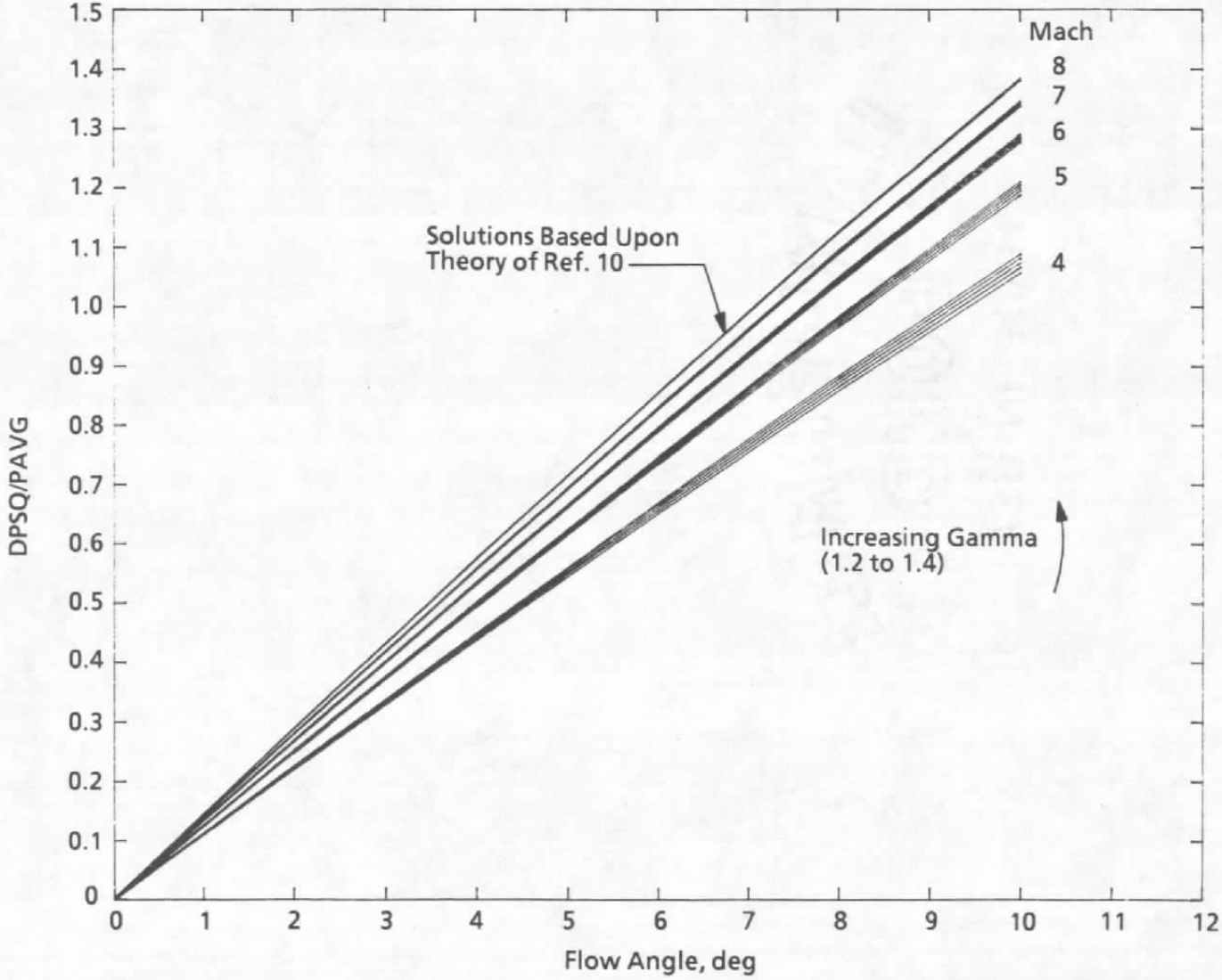

Figure 11. Flow angle probe pressure measurement sensitivity to specific heat ratio.

Notes:
1. All vectors are shown in positive directions.
2. PHI is computed directly from the pressure (see Section 3.2.5)
3. Local Mach number (MLC) and the total angle of attack (AATCA) are computed from curve fits (see Appendix A)
4. Velocity vector components:
   UP/VL = cos (AATCA)
   VP/VL = sin (AATCA) • sin (PHI)
   WP/VL = sin (AATCA) • cos (PHI)

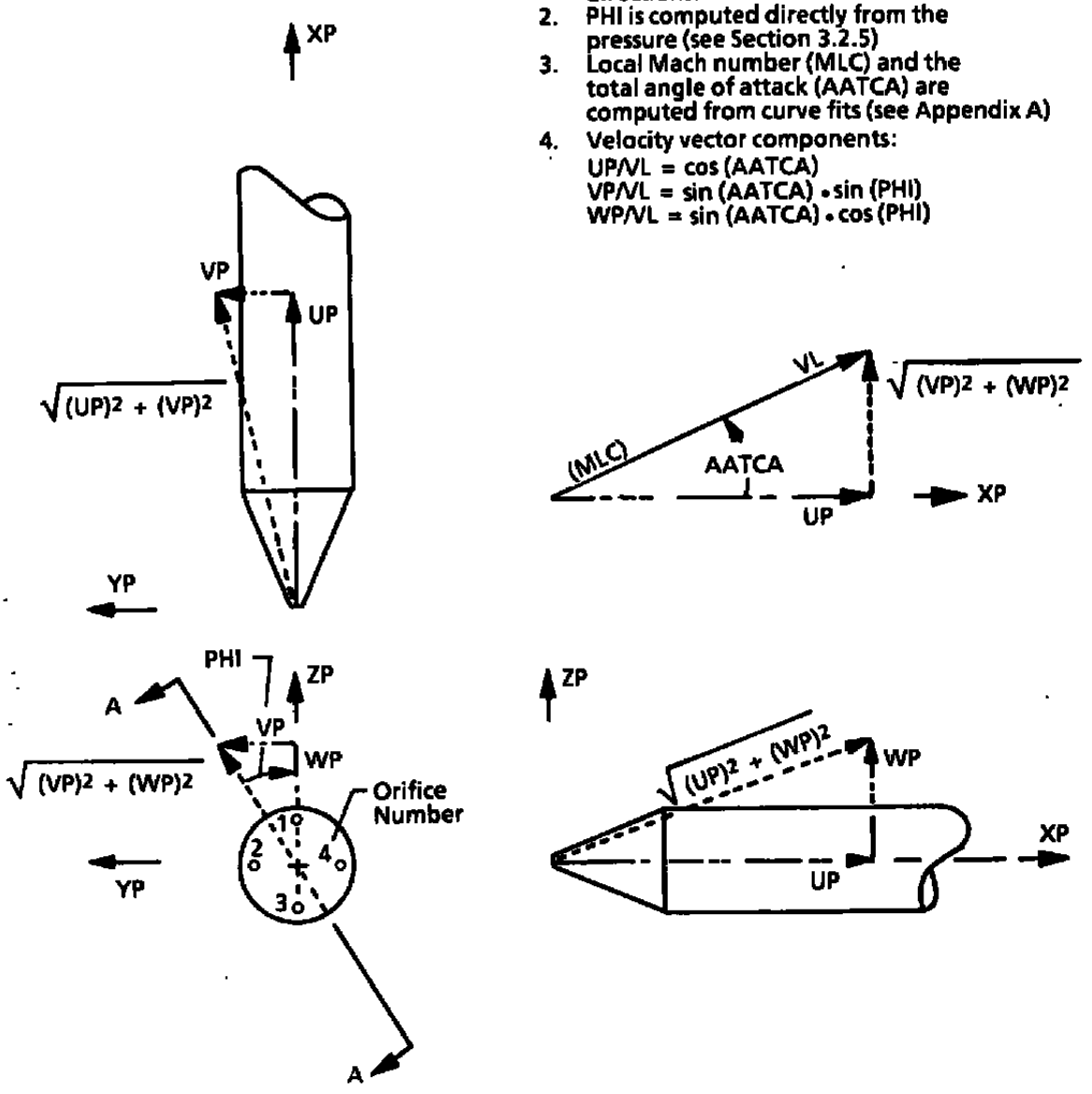

a. With respect to the probe axis system

Figure 12. Flow angle and velocity vector definitions.

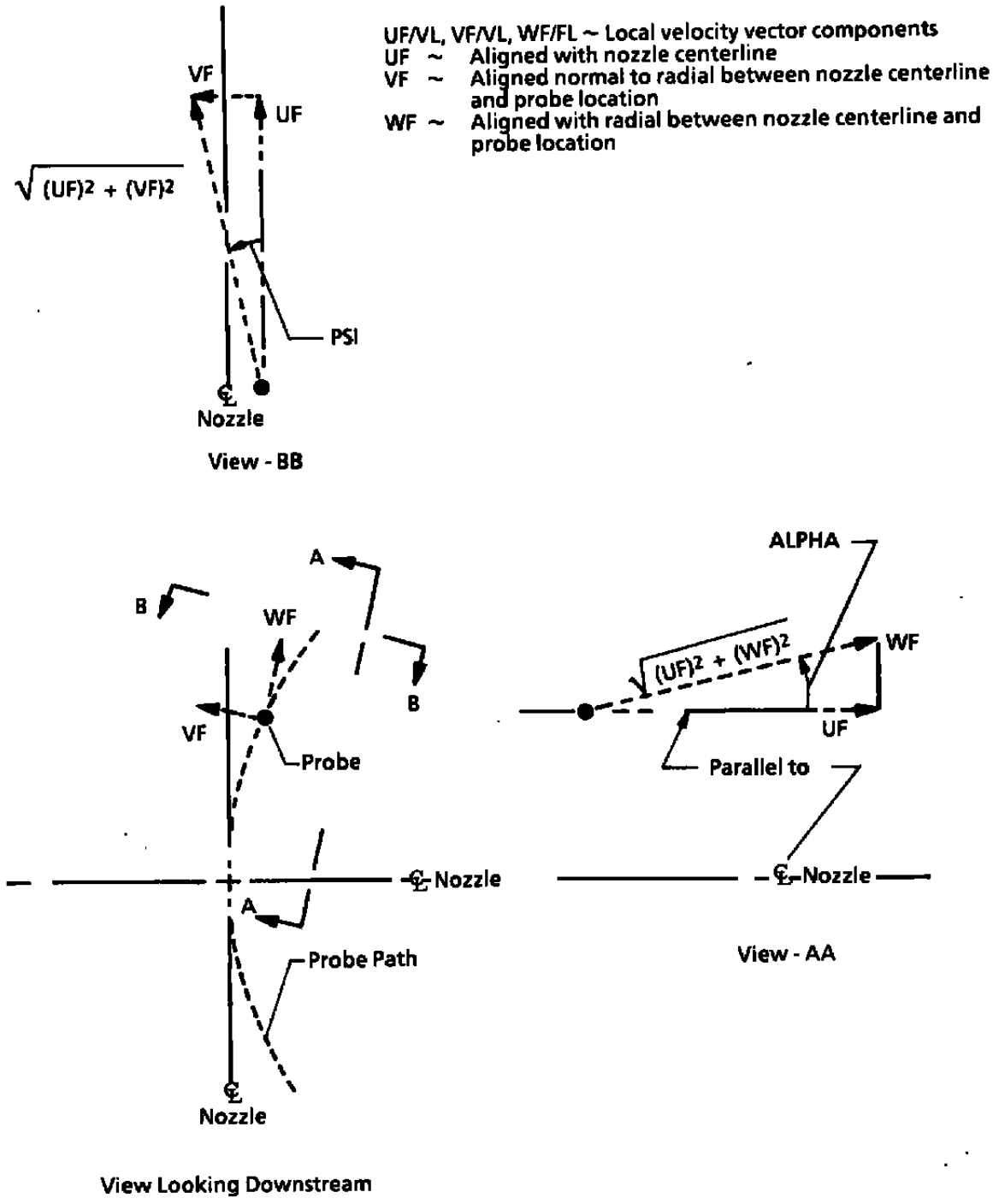

b. With respect to the tunnel axis system
Figure 12. Concluded.

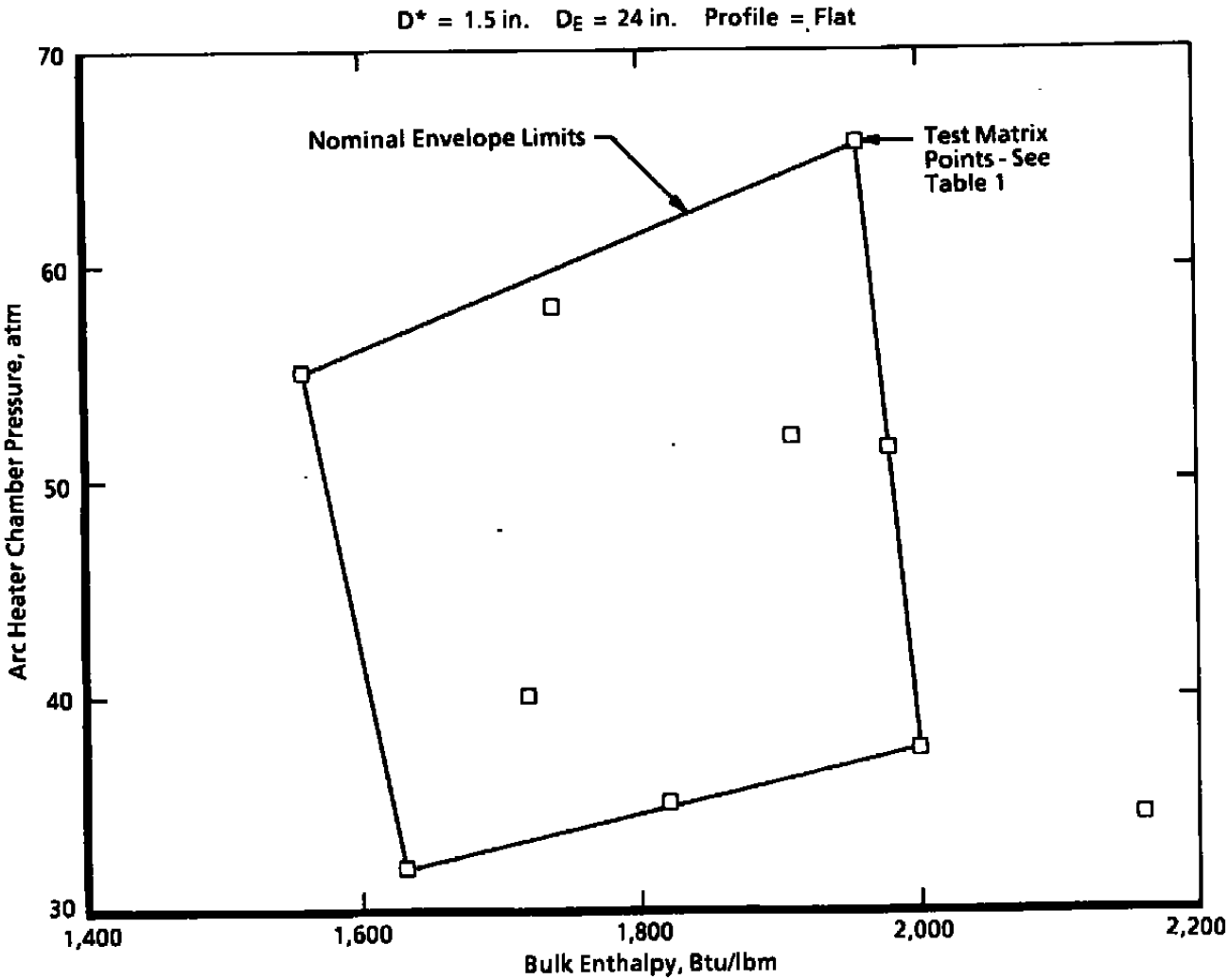

a. Bulk enthalpy–chamber pressure envelope

Figure 13. Demonstrated operating conditions.

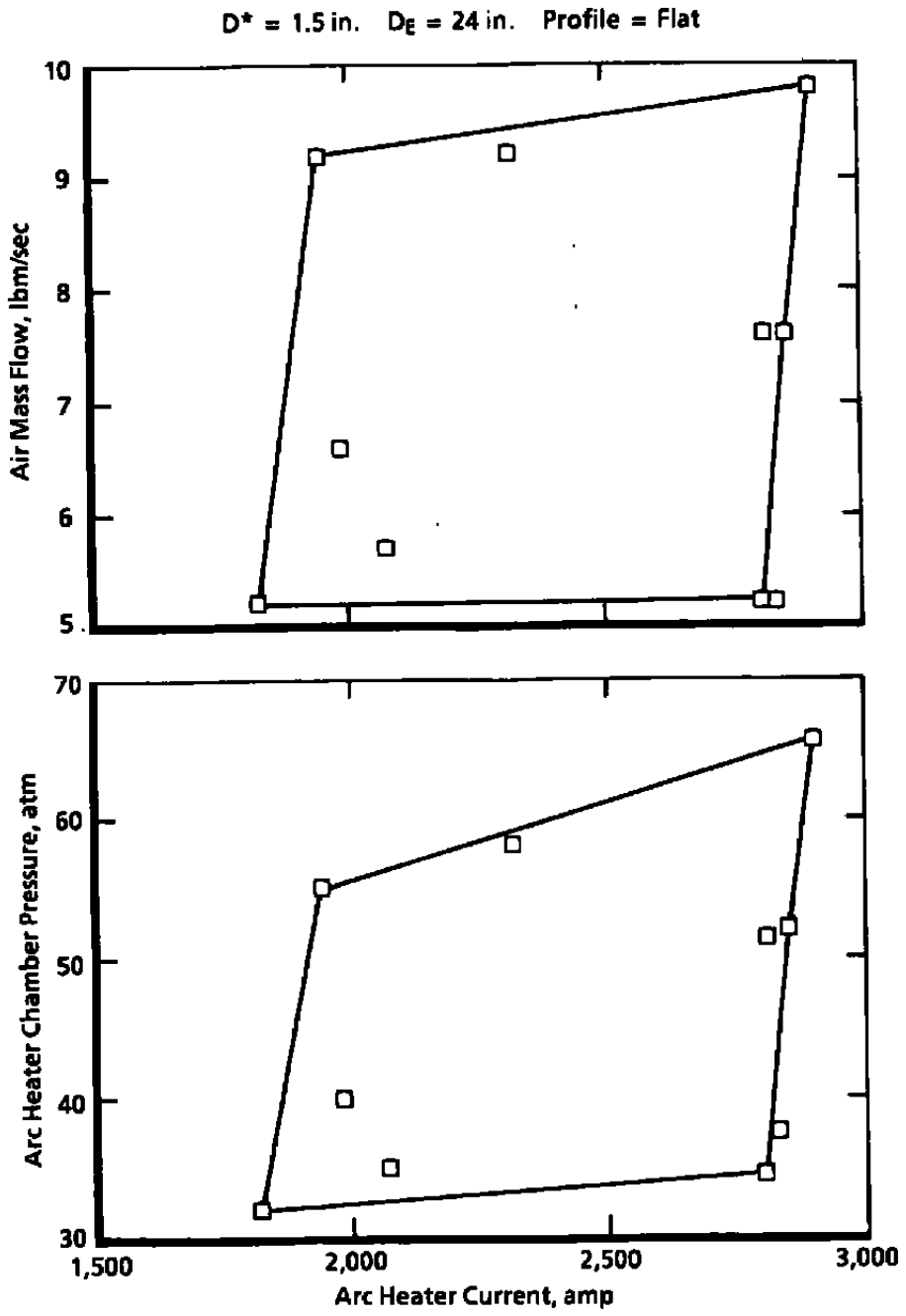

b. Arc current–air mass flow, chamber pressure envelopes
Figure 13. Continued.

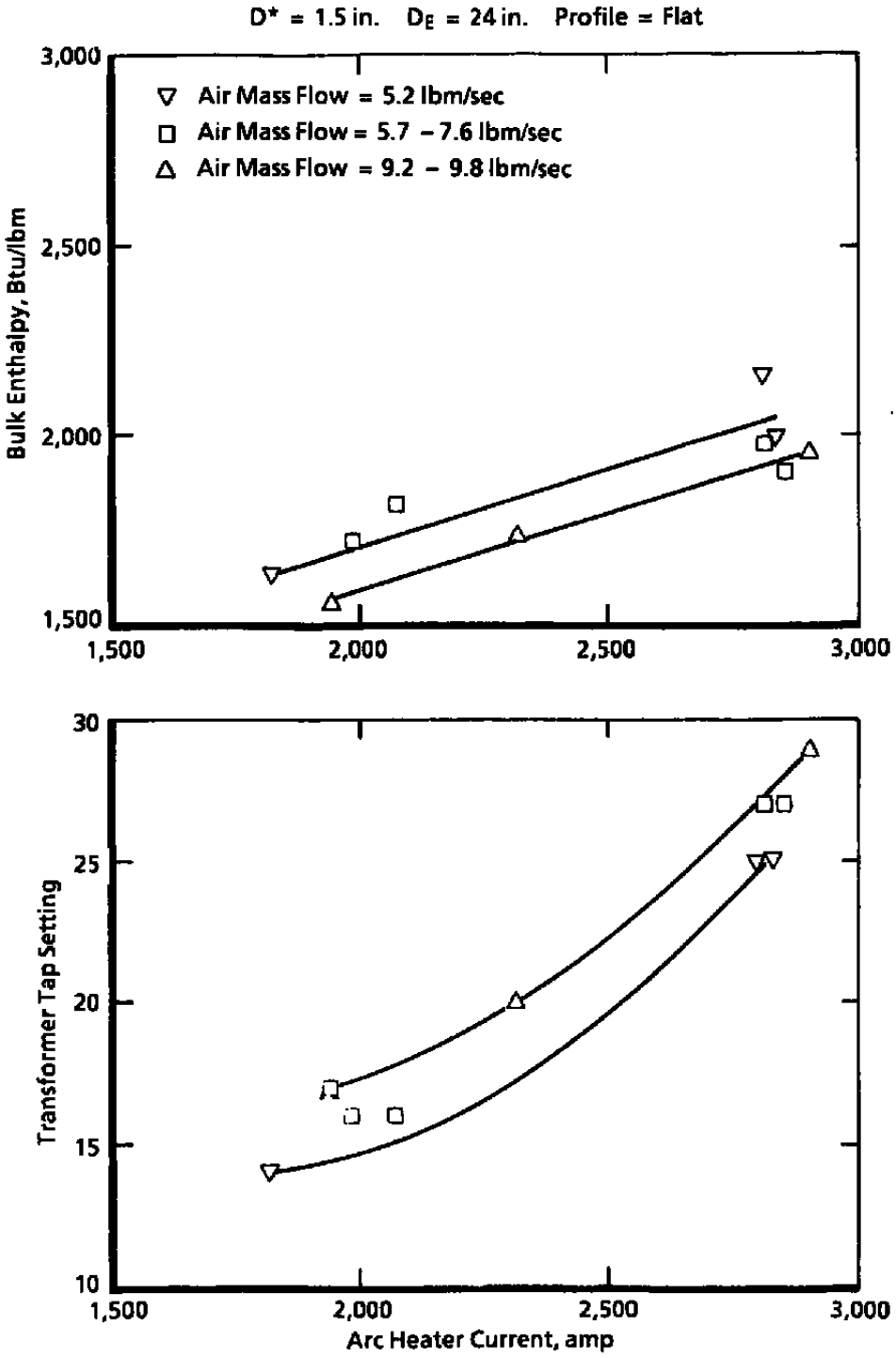

c. Bulk enthalpy, transformer tap setting relationship

Figure 13. Continued.

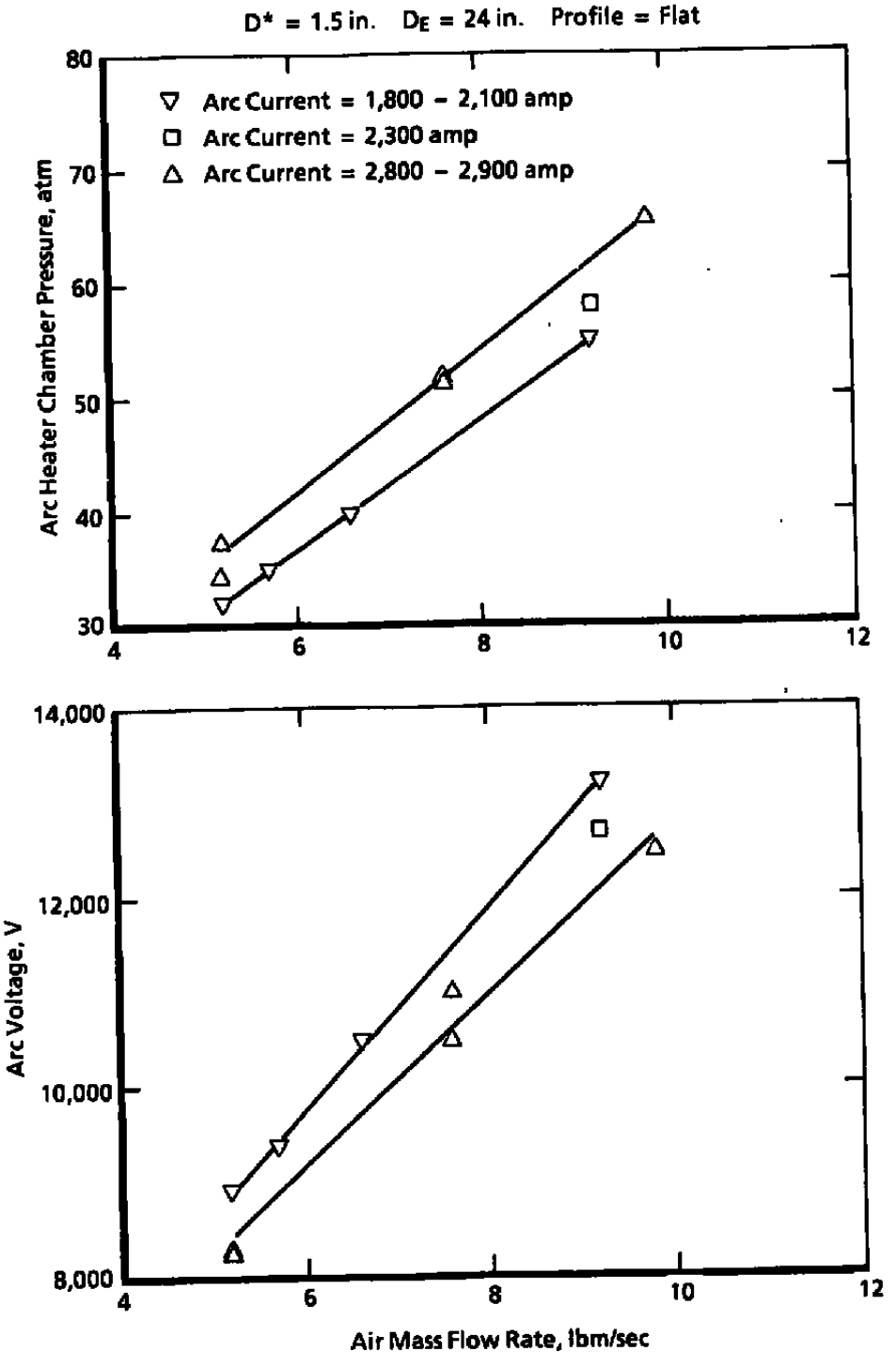

d. Chamber pressure, voltage relationships

Figure 13. Concluded.

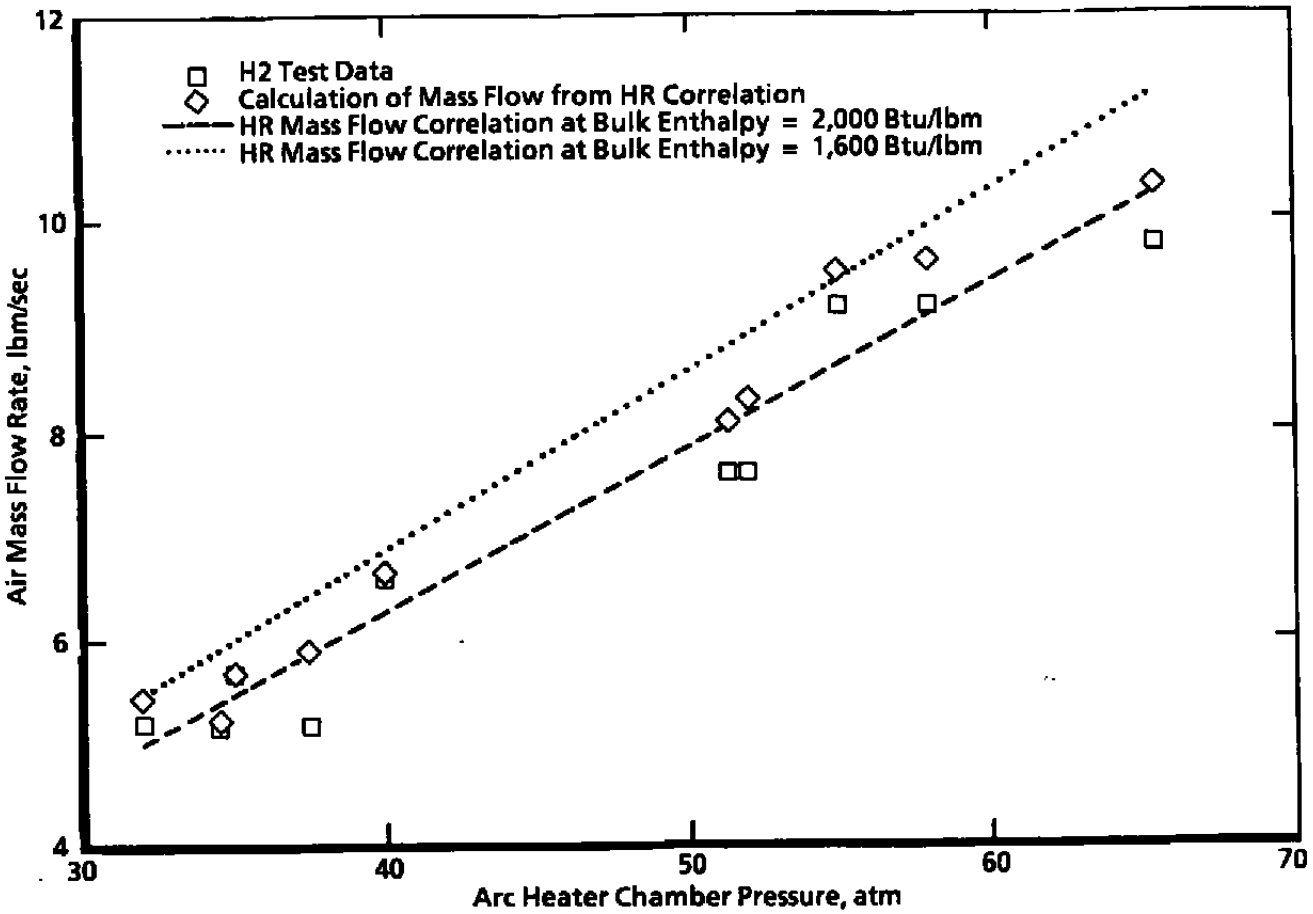

a. Air mass flow rate based on arc chamber pressure

Figure 14. HEAT-H2 operating data to HEAT-HR correlation comparison.

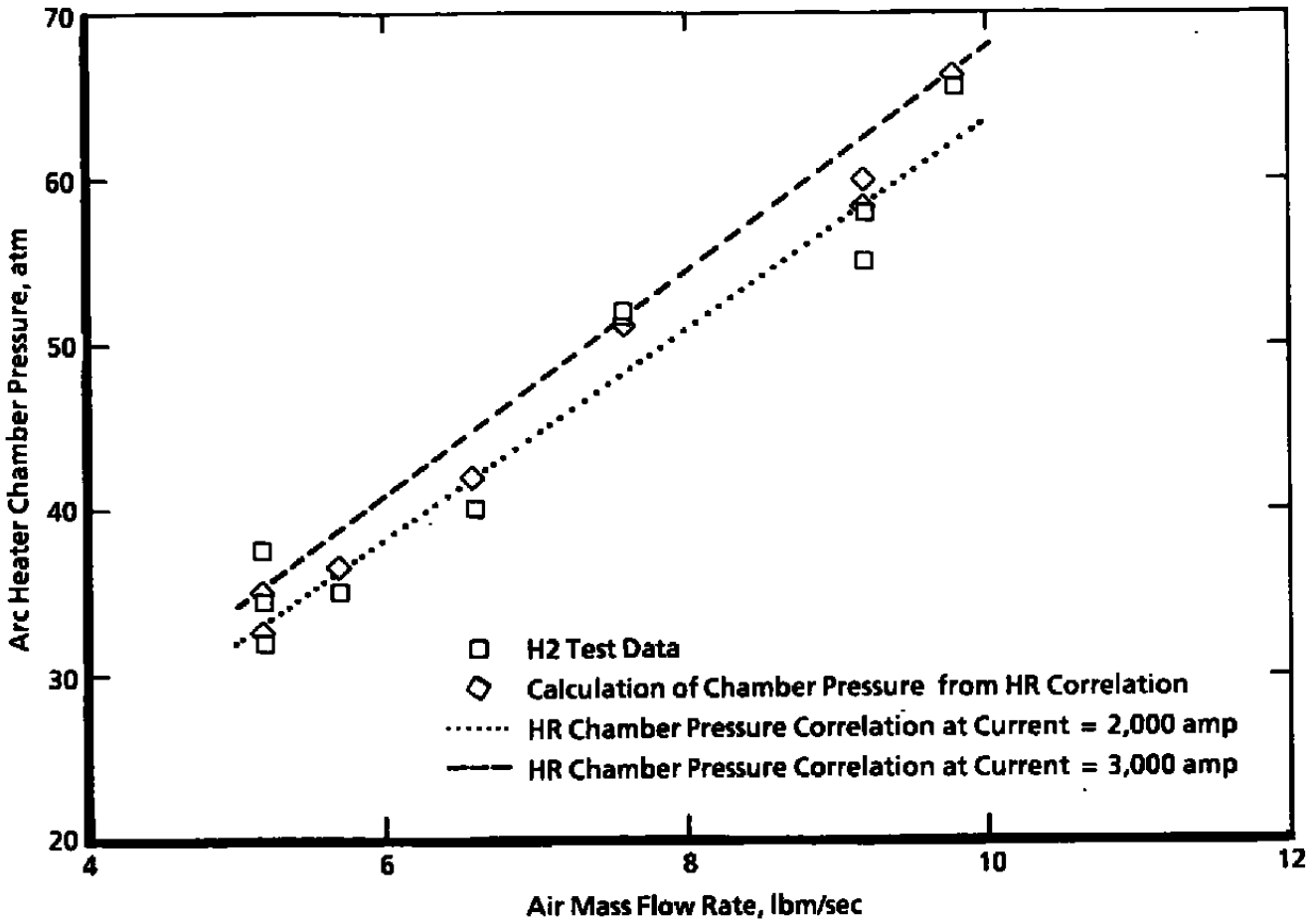

b. Arc heater chamber pressure based on air mass flow
Figure 14. Continued.

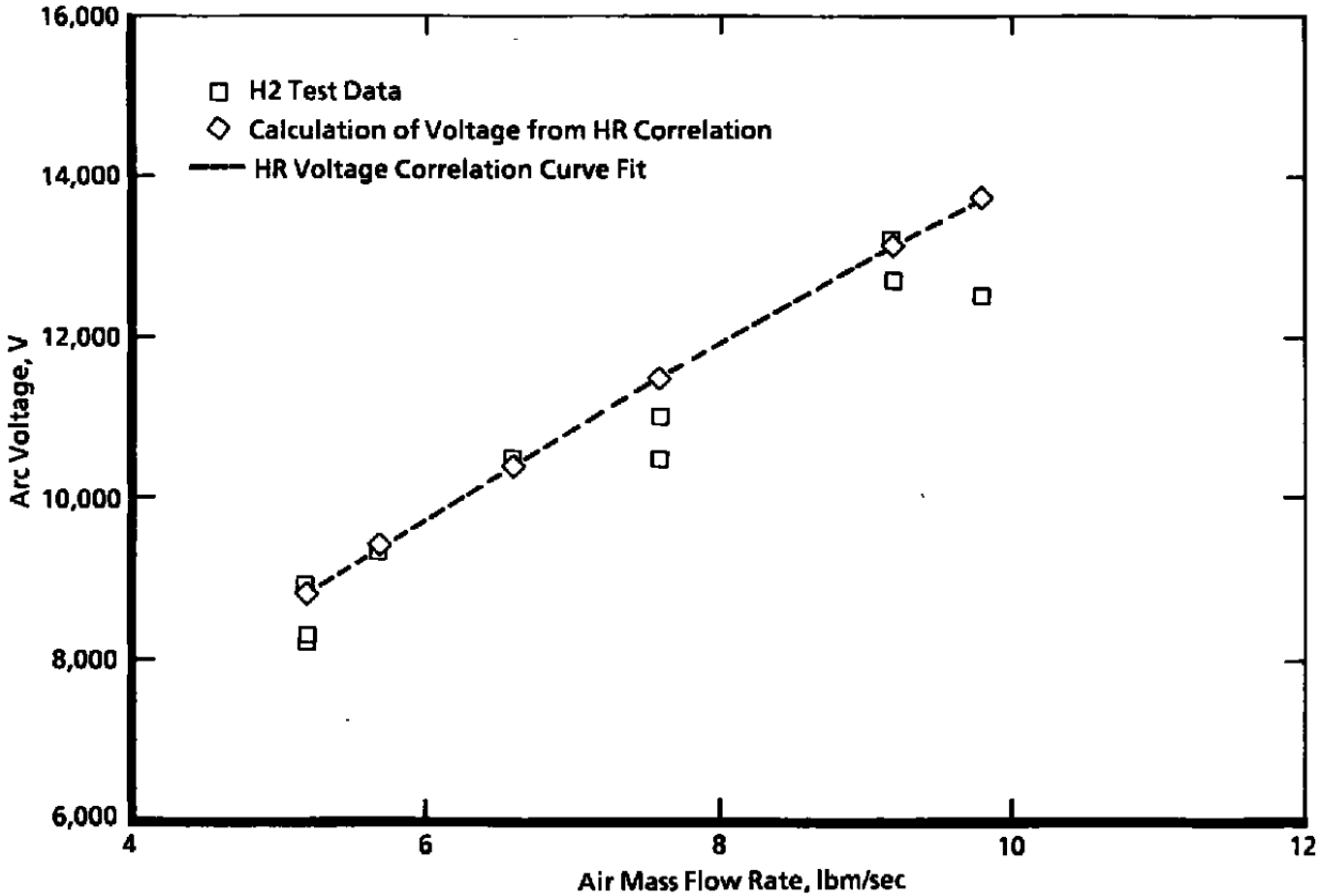

c. Arc voltage based on air mass flow rate

Figure 14. Concluded.

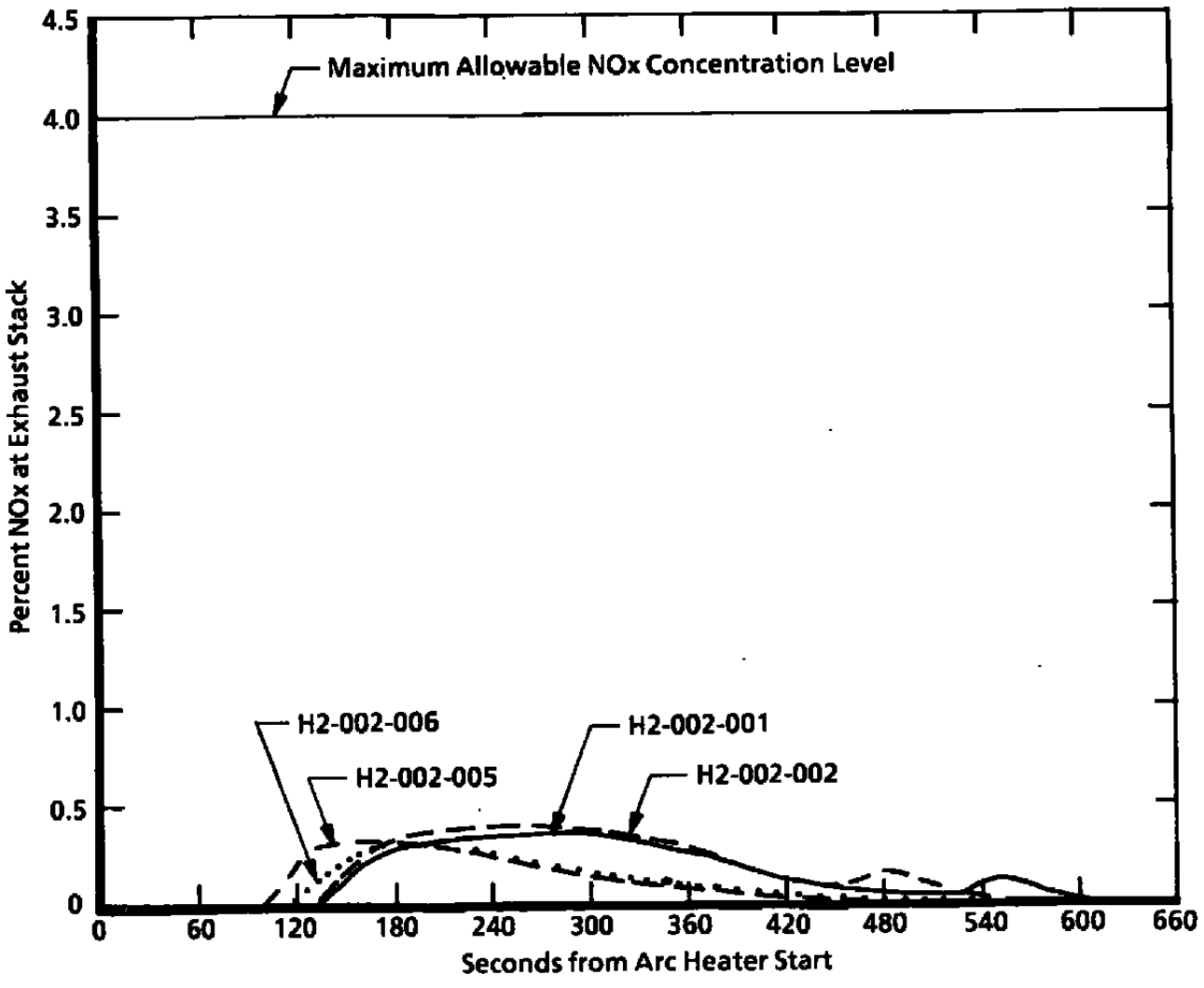

Figure 15. Exhaust stack measurements.

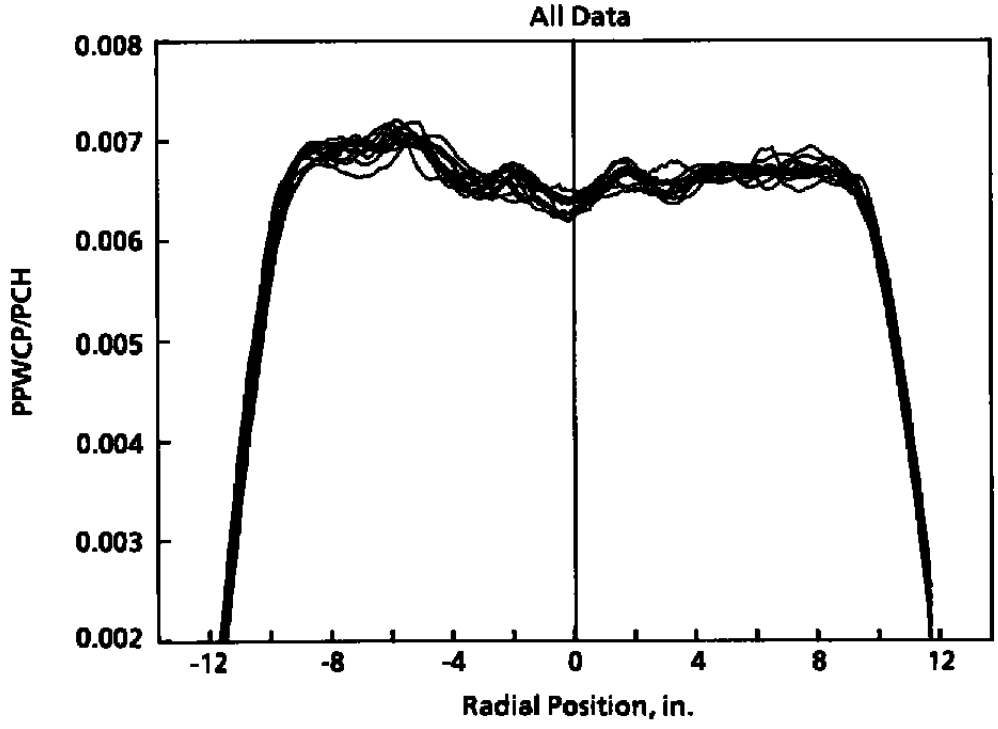

a. XO = 2

Figure 16. Pitot pressure profiles.

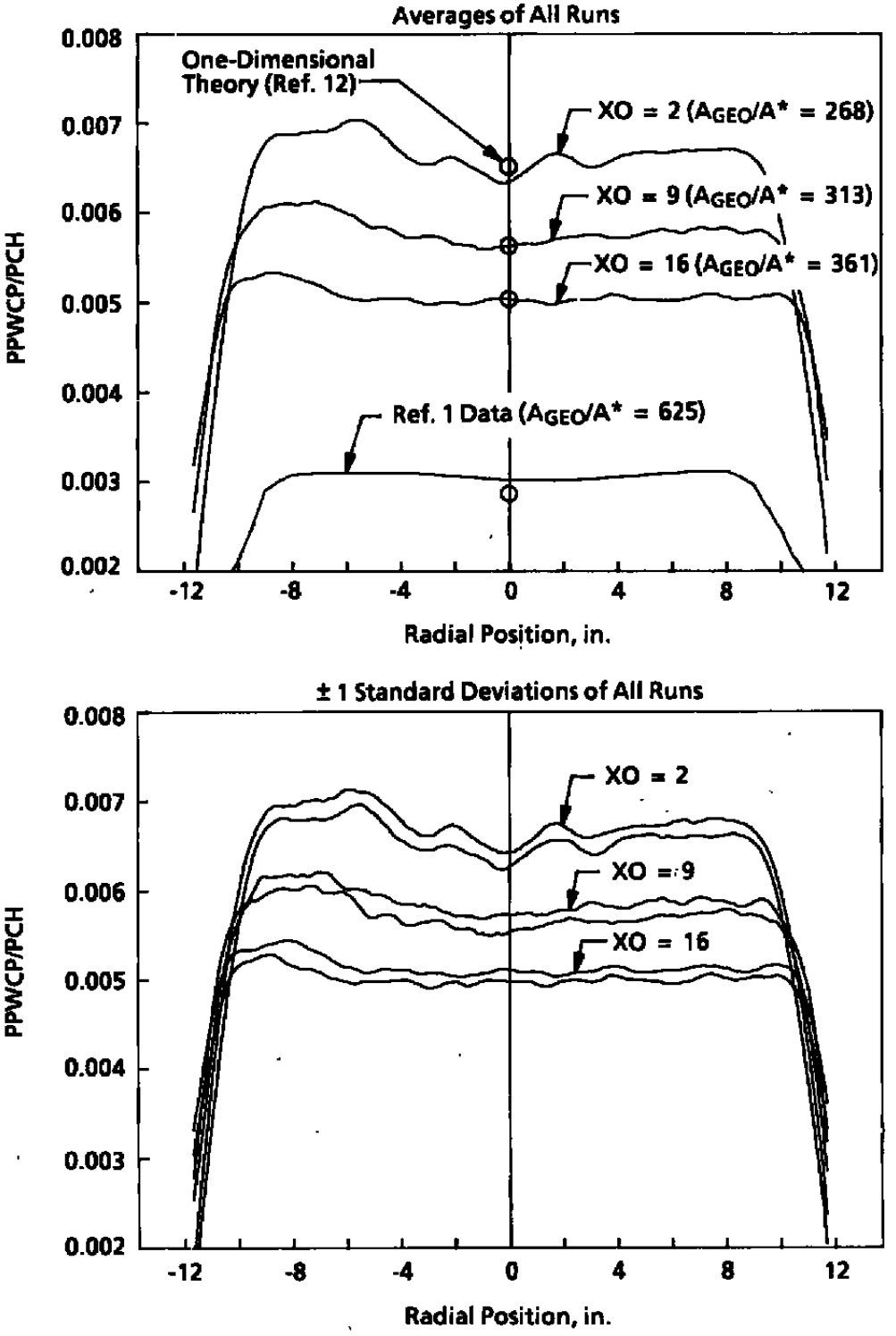

b. Averages and standard deviations at XO = 2, 9, and 16

Figure 16. Concluded.

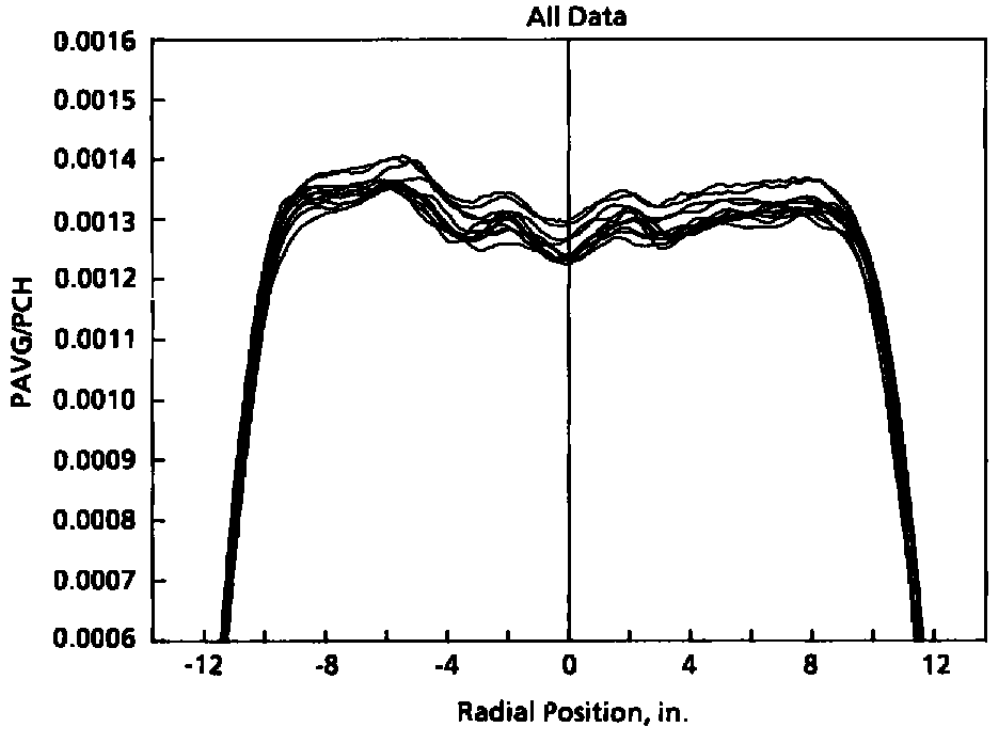

a. XO = 2

Figure 17. Flow angle probe surface pressure profiles.

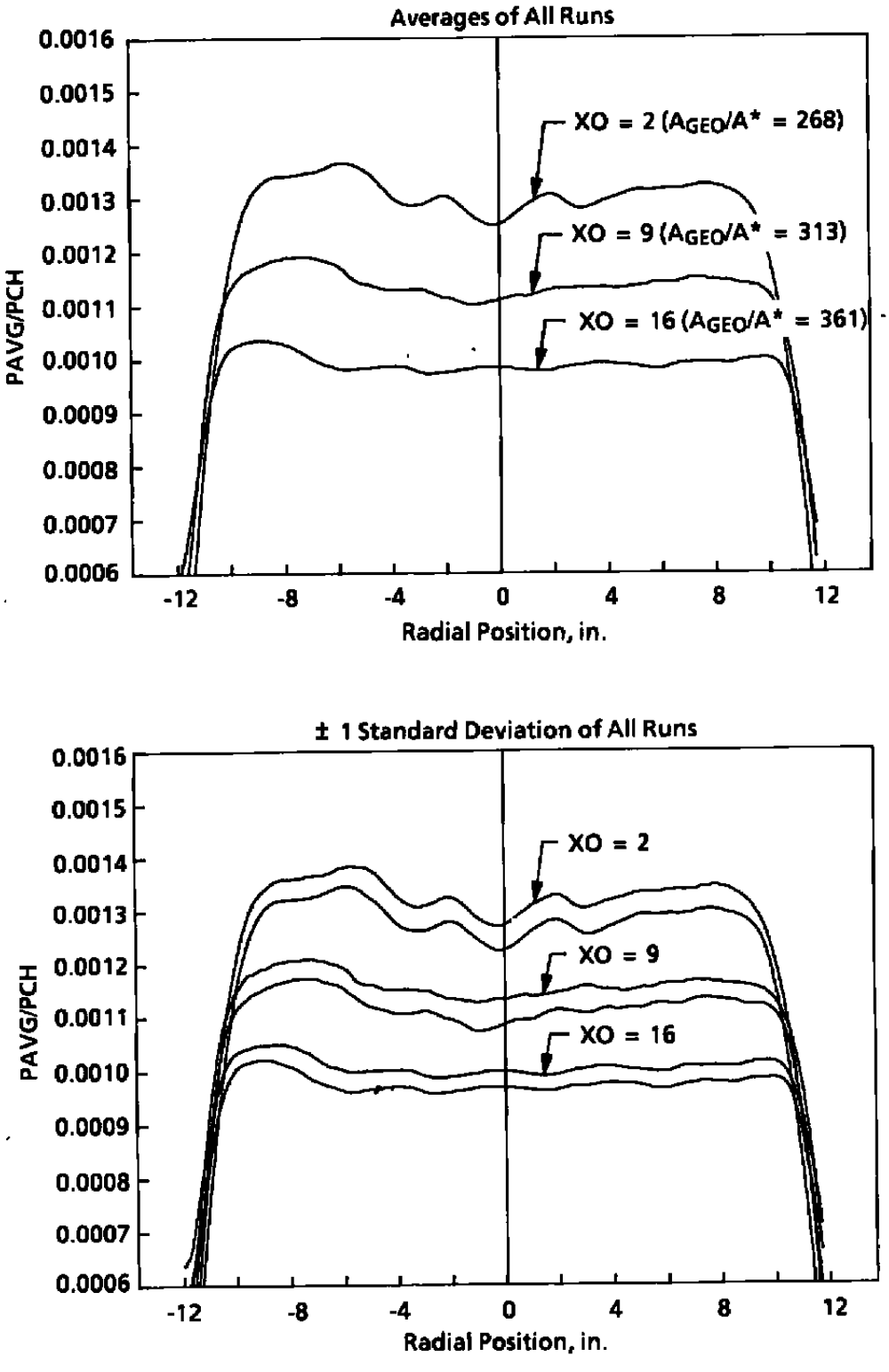

b. Averages and standard deviation at XO = 2, 9, and 16

Figure 17. Concluded.

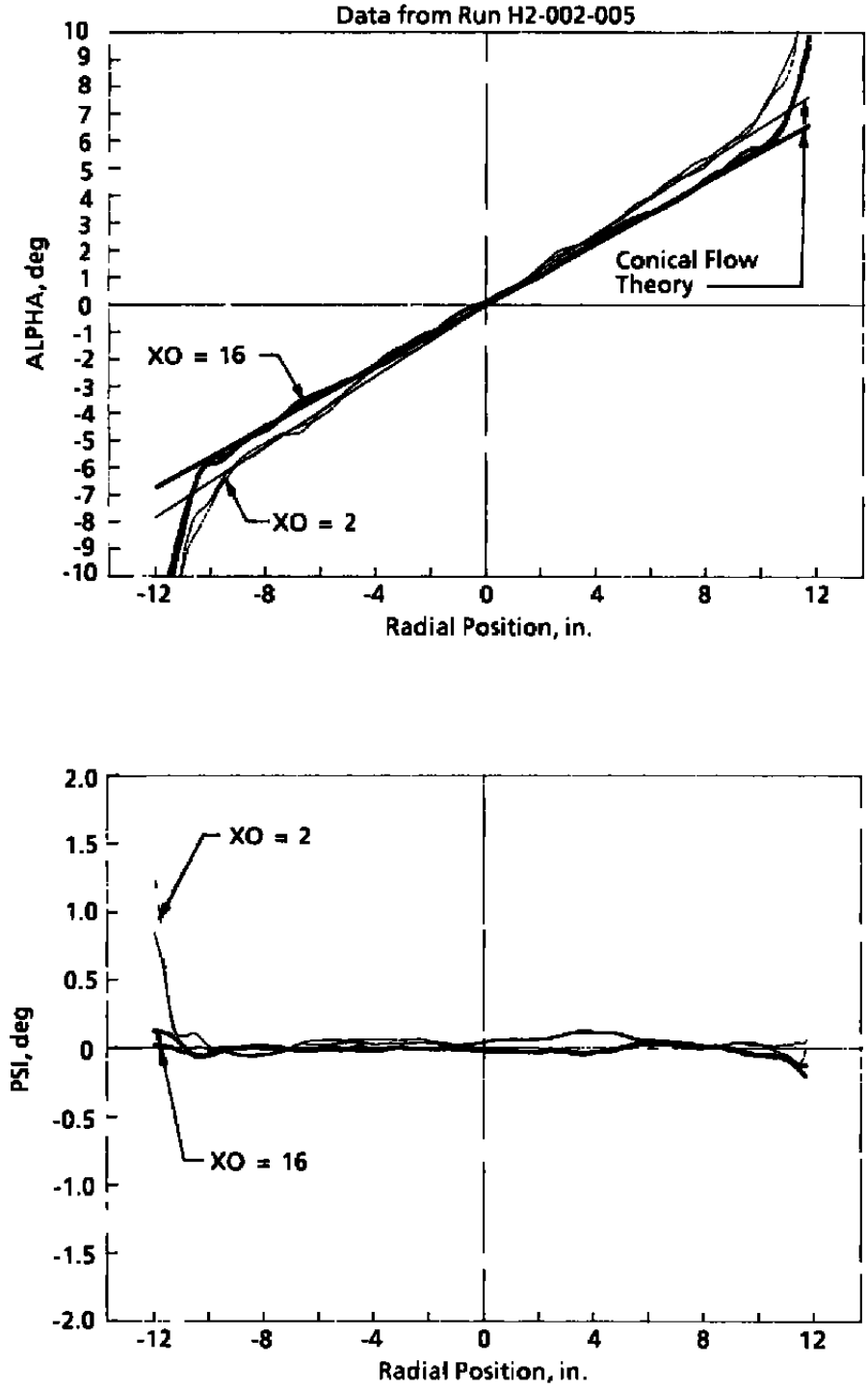

a. Flow divergence and circumferential flow angle about nozzle centerline

Figure 18. Typical flow angularity profiles.

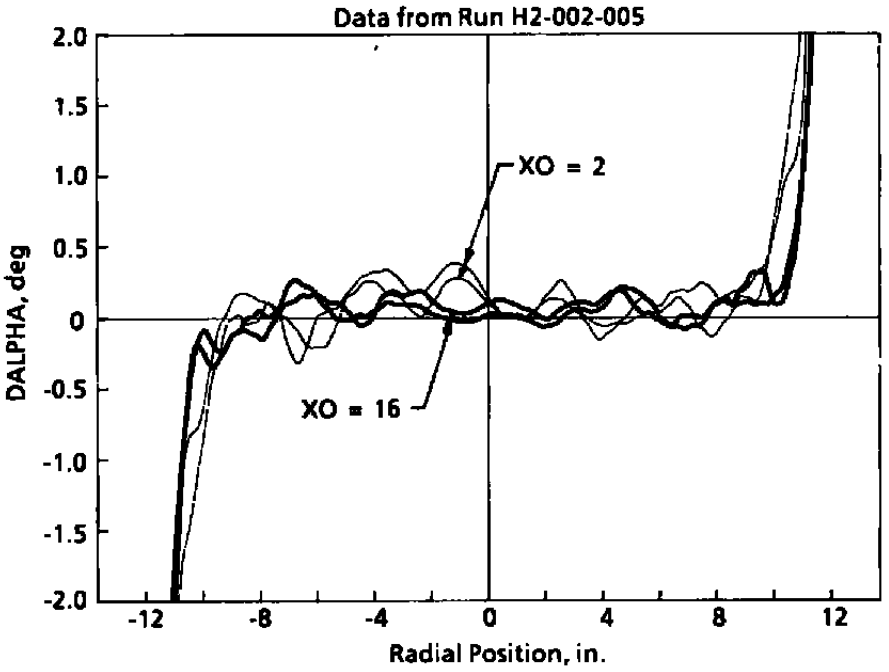

b. Deviations from conical theory
Figure 18. Concluded.

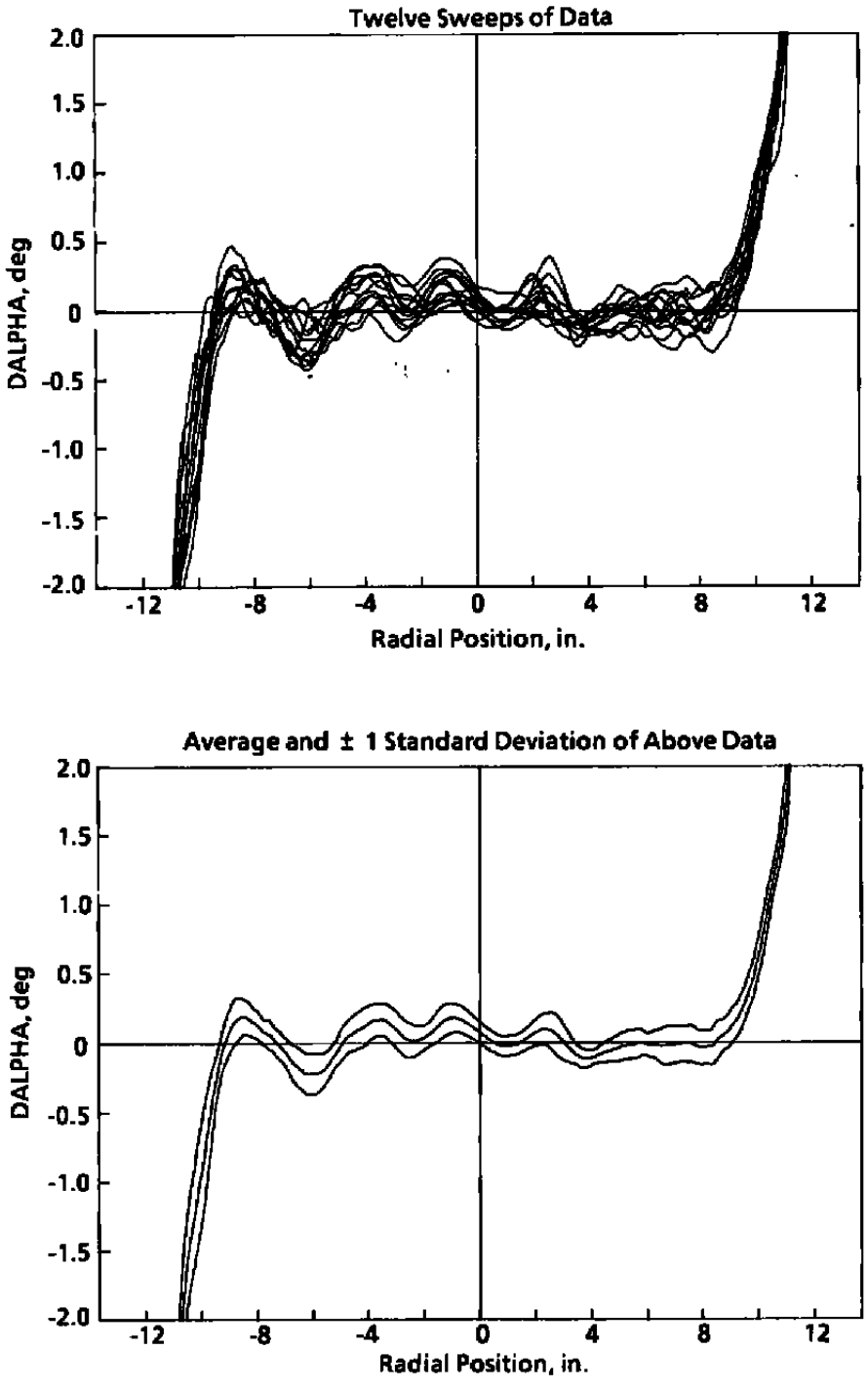

a. XO = 2

Figure 19. Flow divergence, deviation from conical theory.

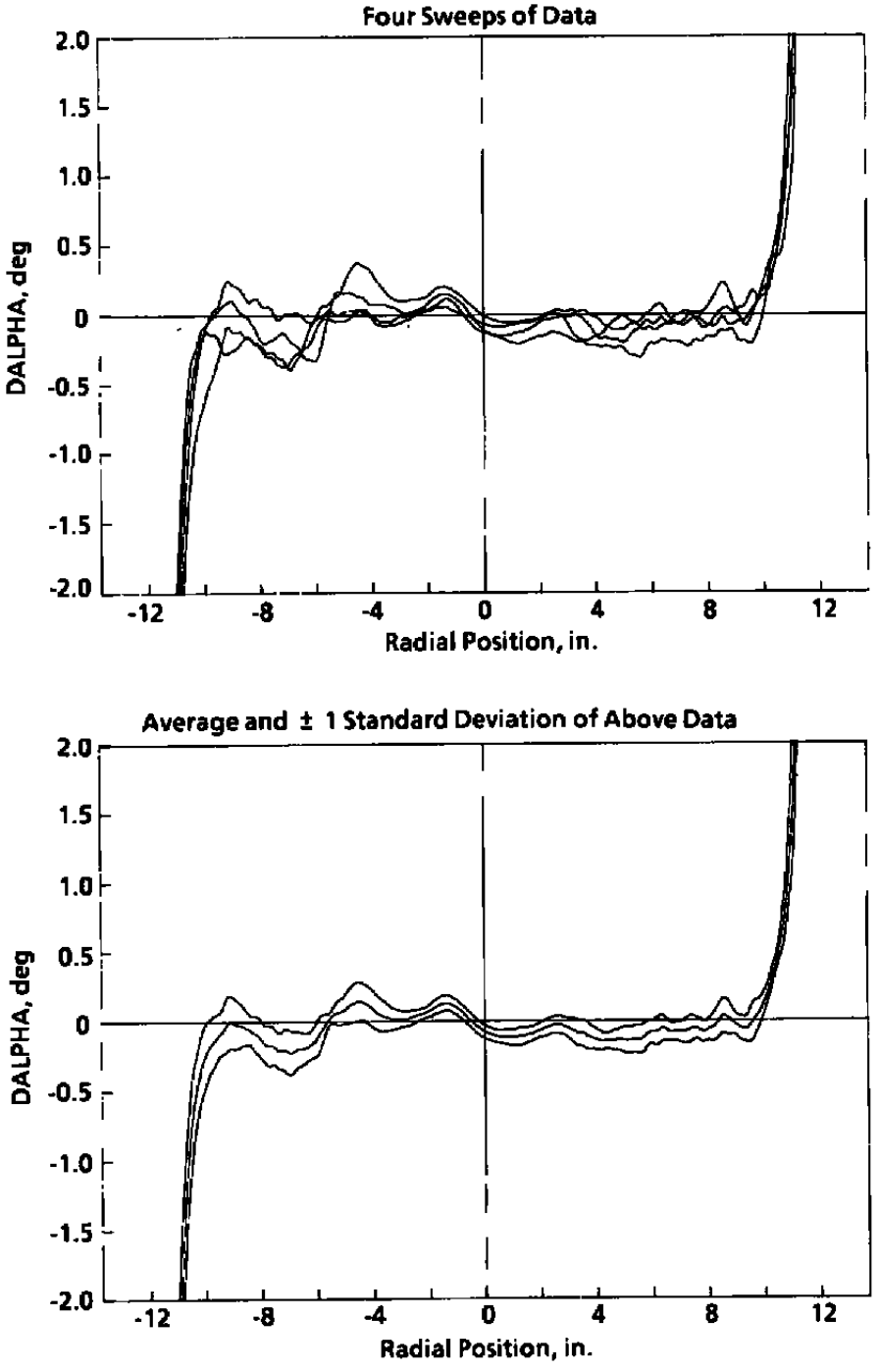

b. XO = 9

Figure 19. Continued.

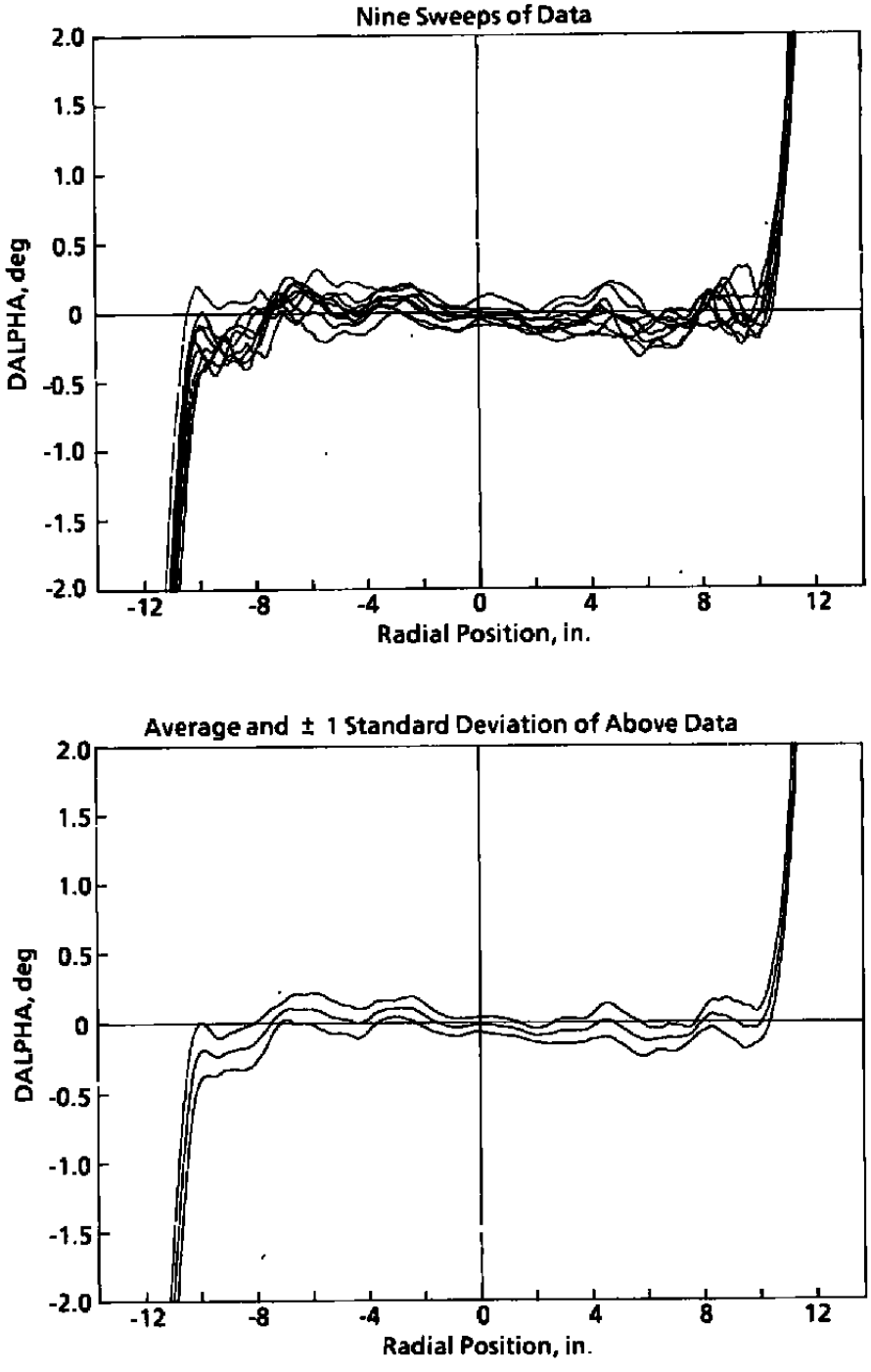

c. XO = 16

Figure 19. Concluded.

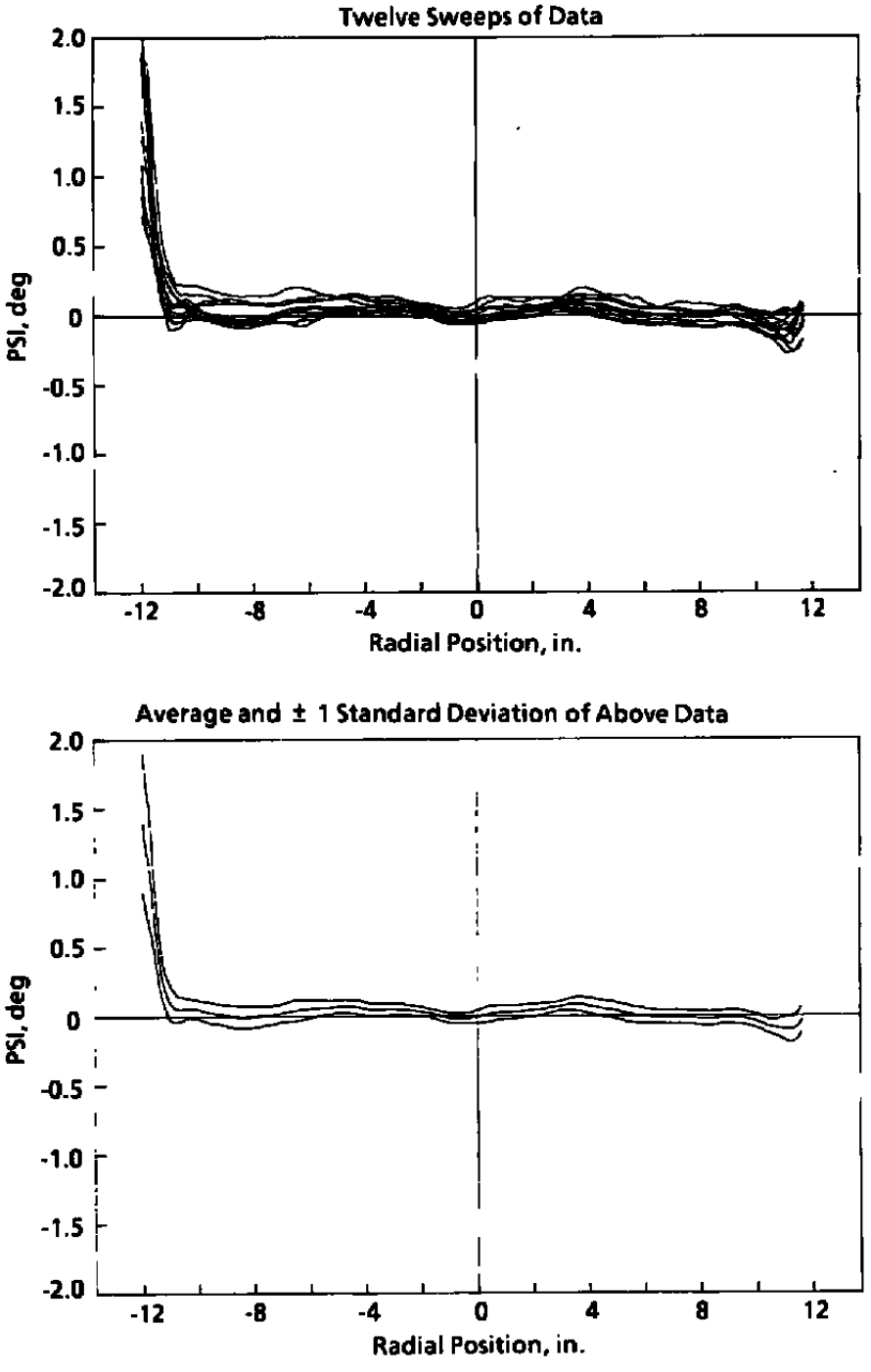

a. XO = 2

Figure 20. Flow circulation.

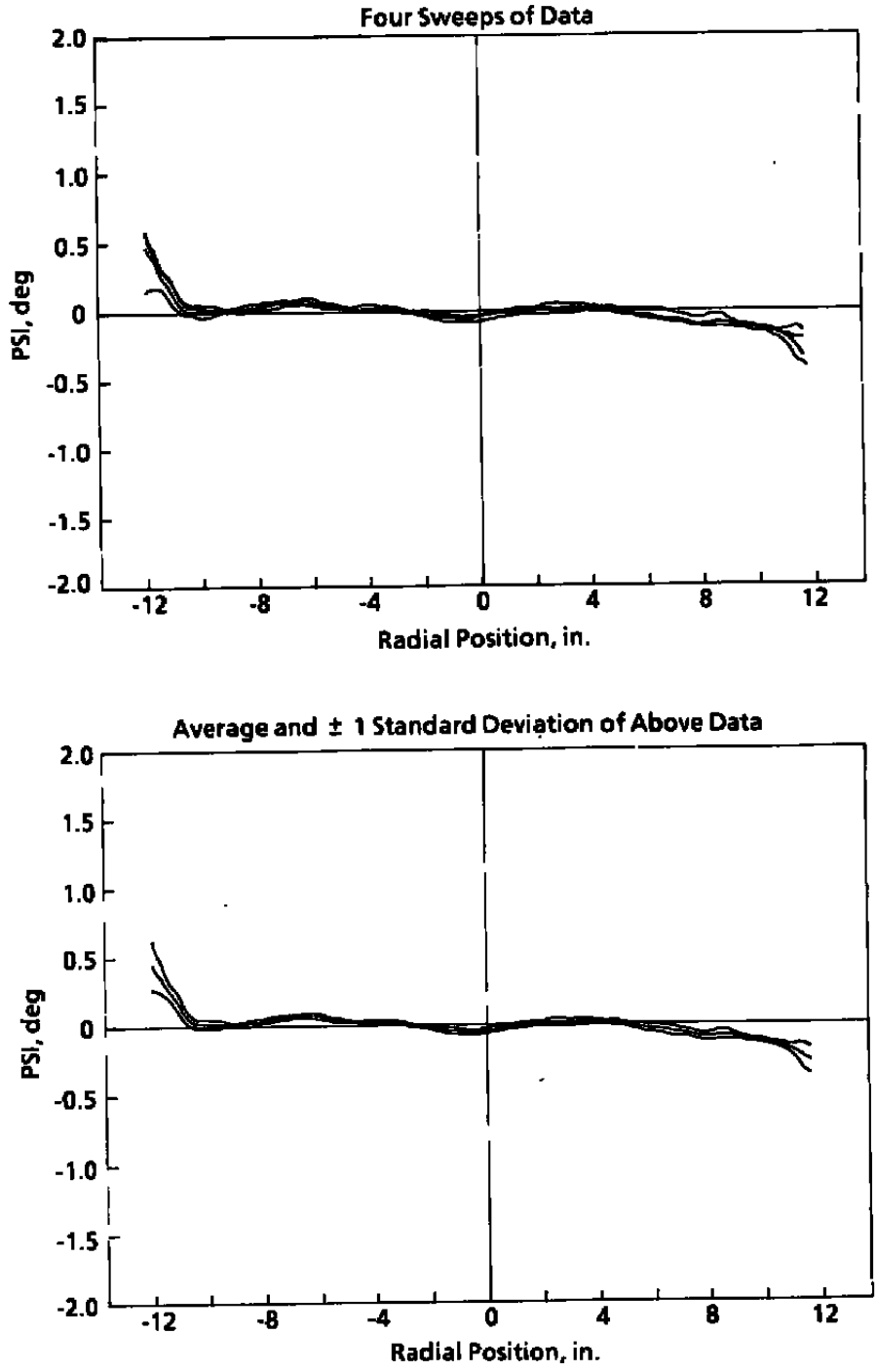

b. XO = 9

Figure 20. Continued.

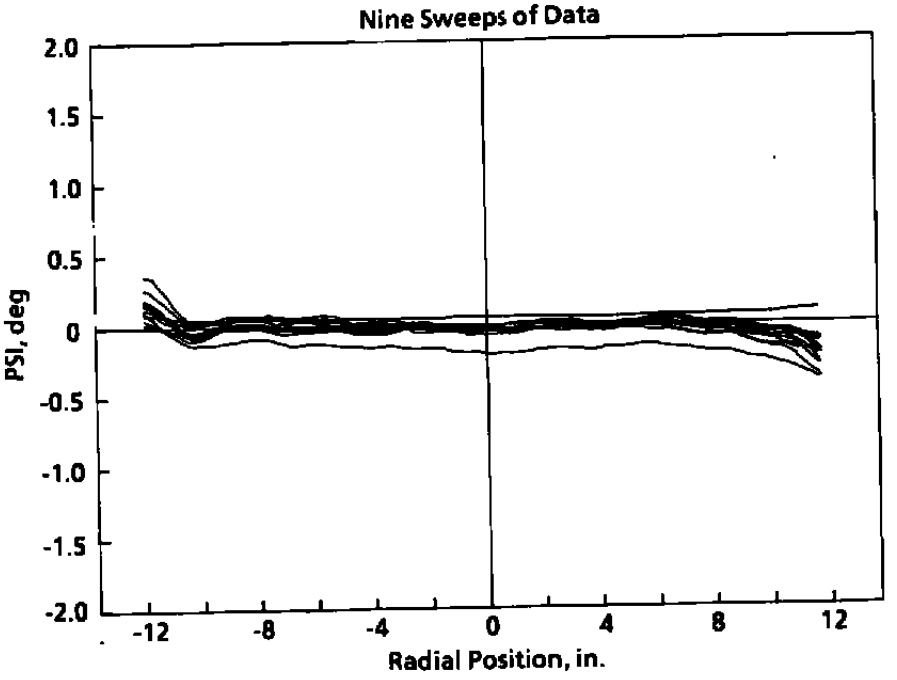

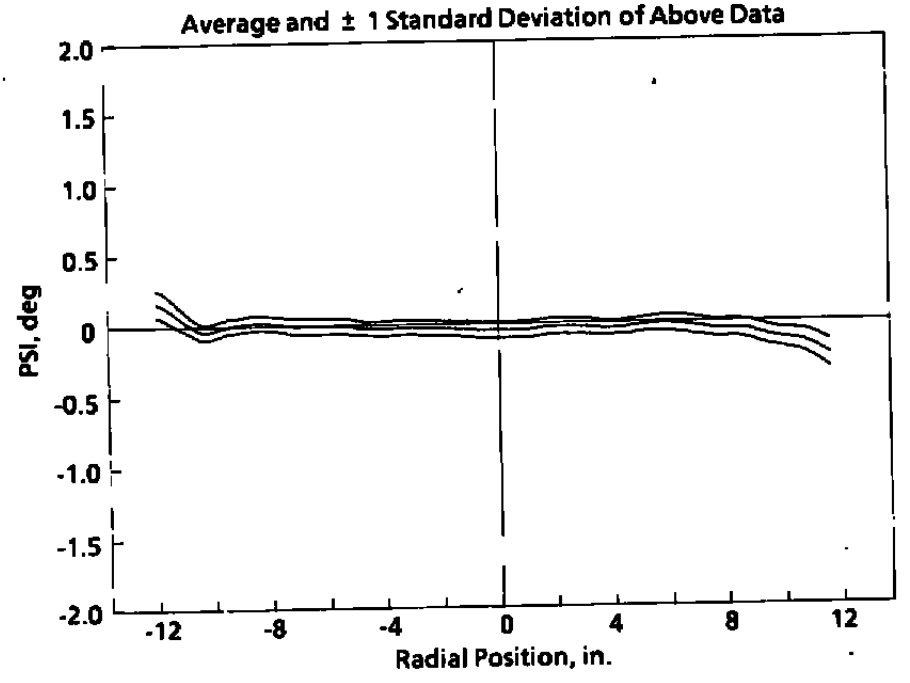

c. XO = 16

Figure 20. Concluded.

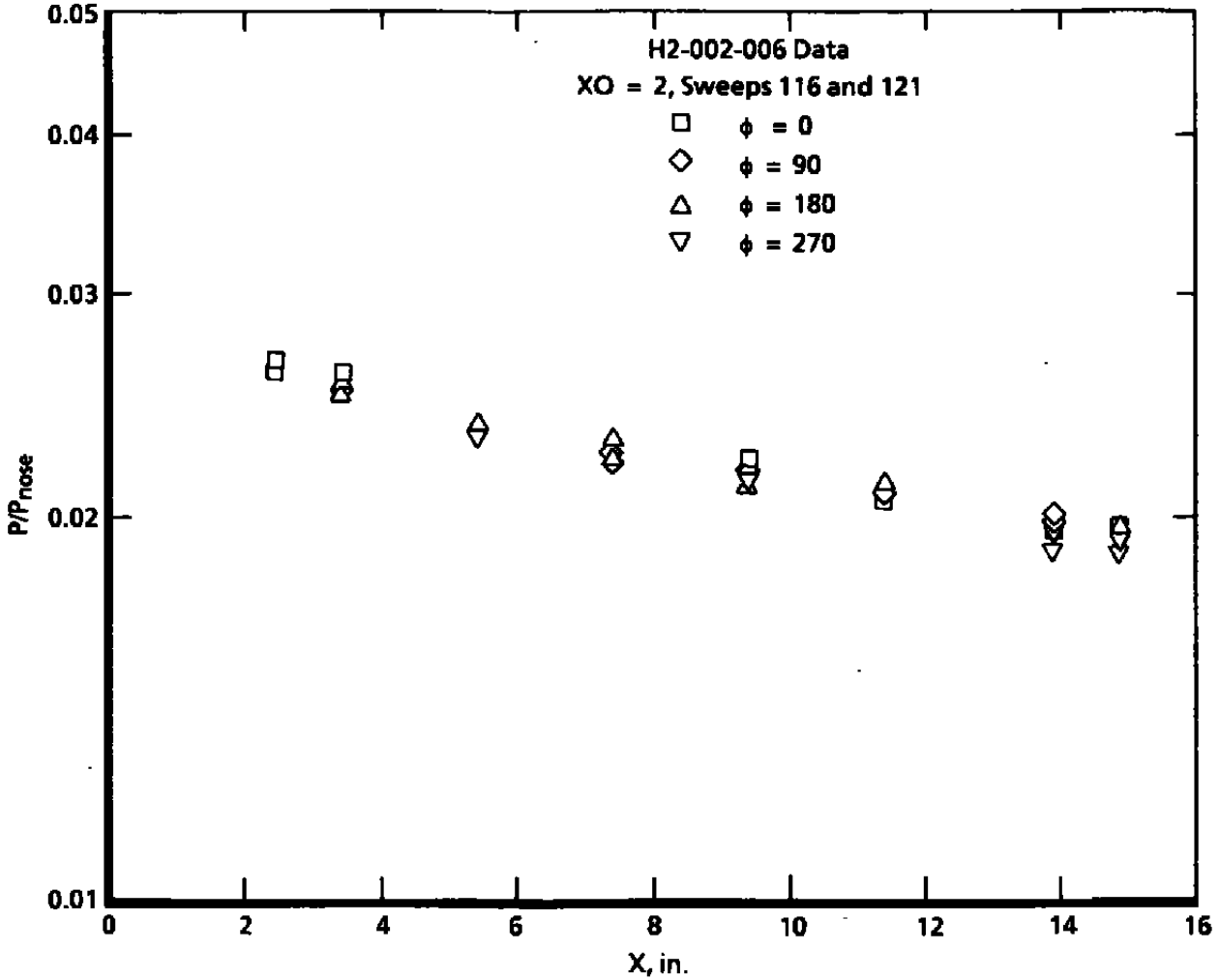

a. Circumferential variation and repeatability

Figure 21. Blunt cone surface pressure distributions.

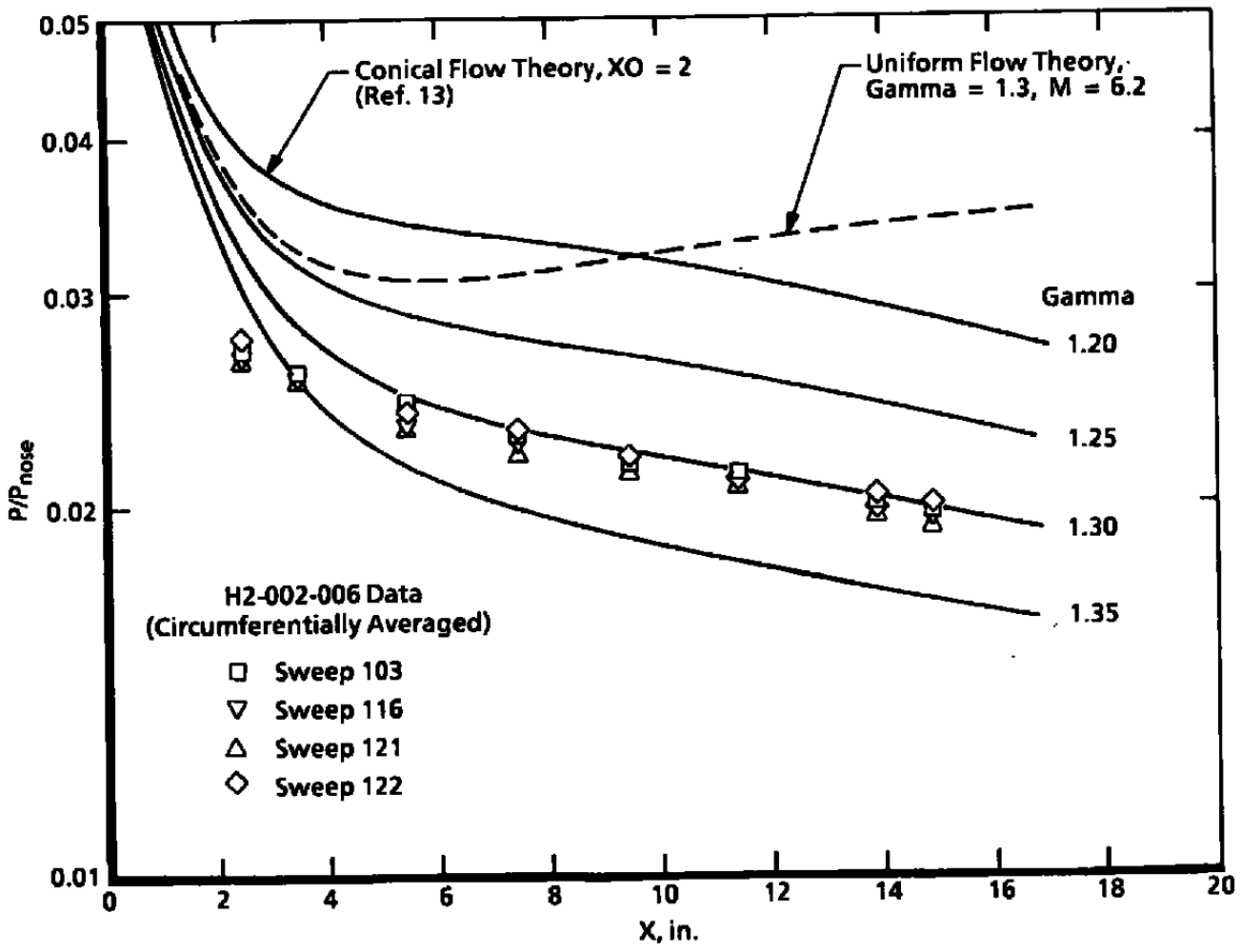

b. Comparison of XO = 2 data with theory

Figure 21. Continued.

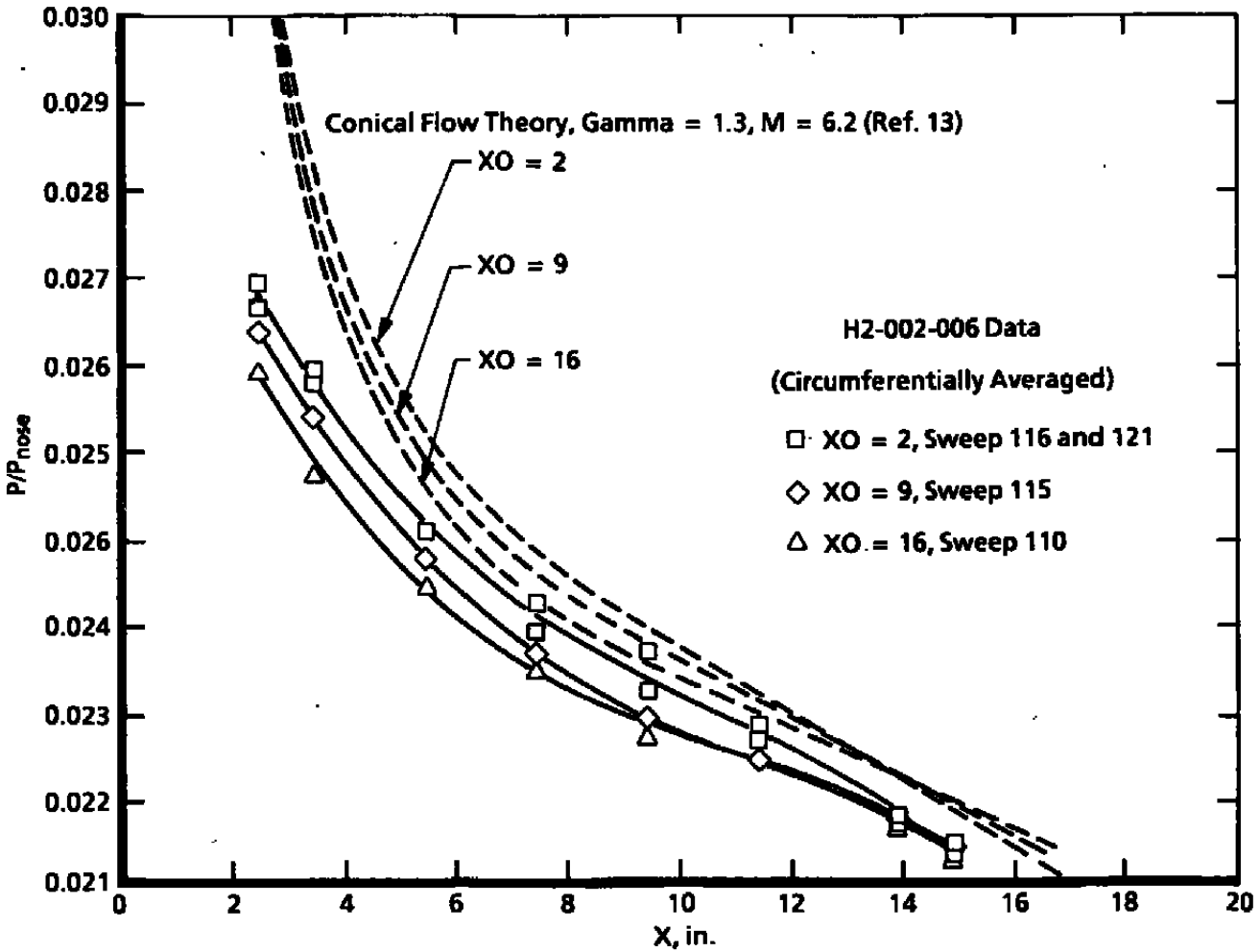

c. Data at XO = 2, 9, 16 compared with theory

Figure 21. Concluded.

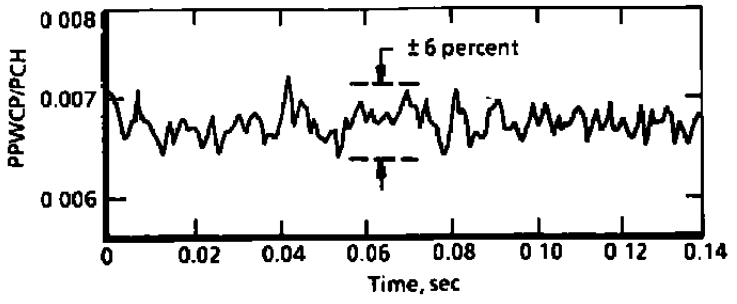

a. Typical pressure-time trace

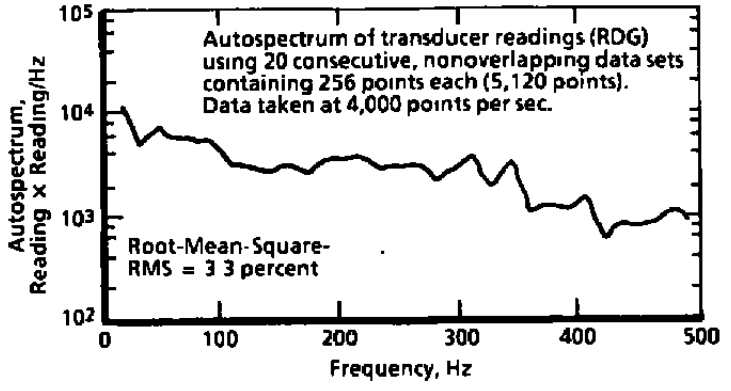

b. Autospectrum of transducer readings

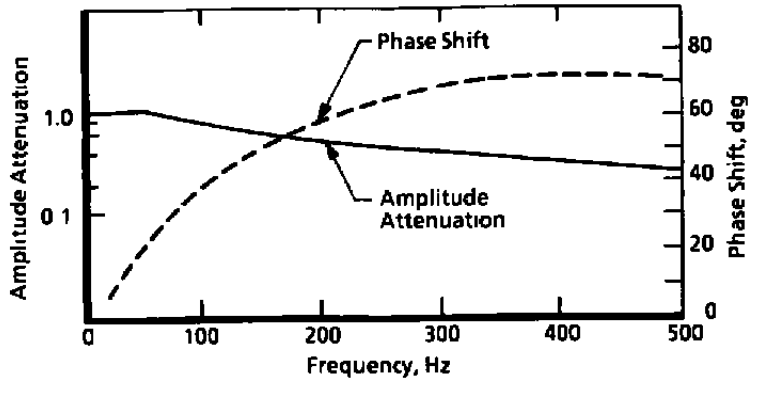

c. Measurement response characteristics

Figure 22. Temporal pitot pressure data, XO = 2.

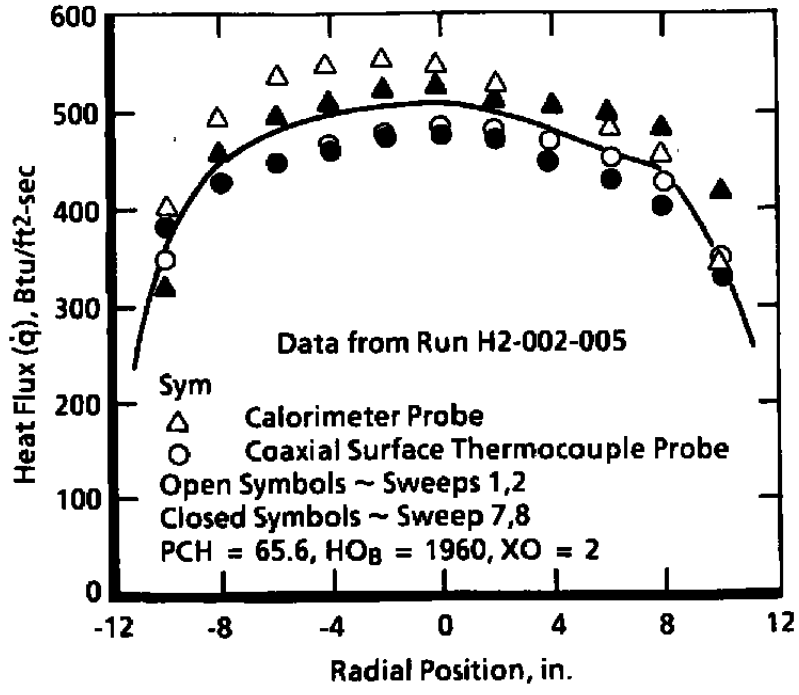

a. Heat flux

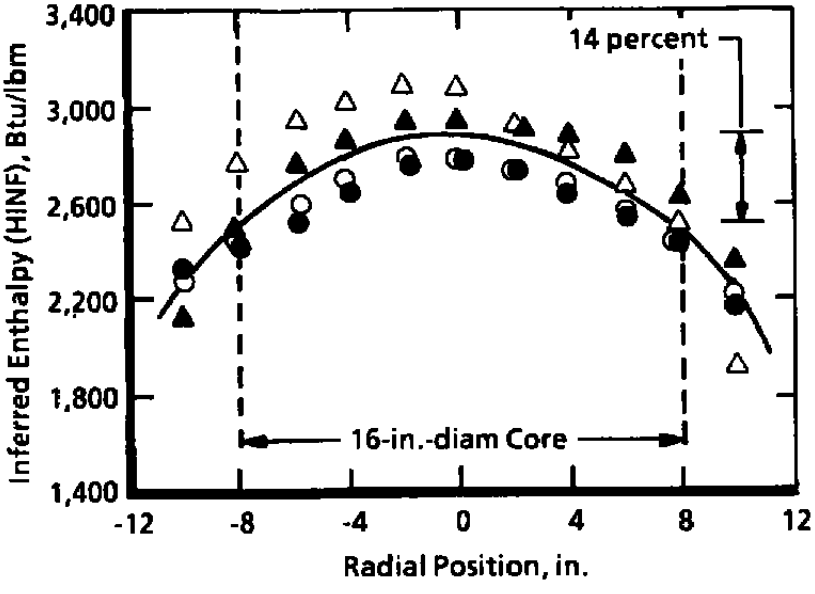

b. Inferred enthalpy

Figure 23. Heat flux and inferred enthalpy repeatability.

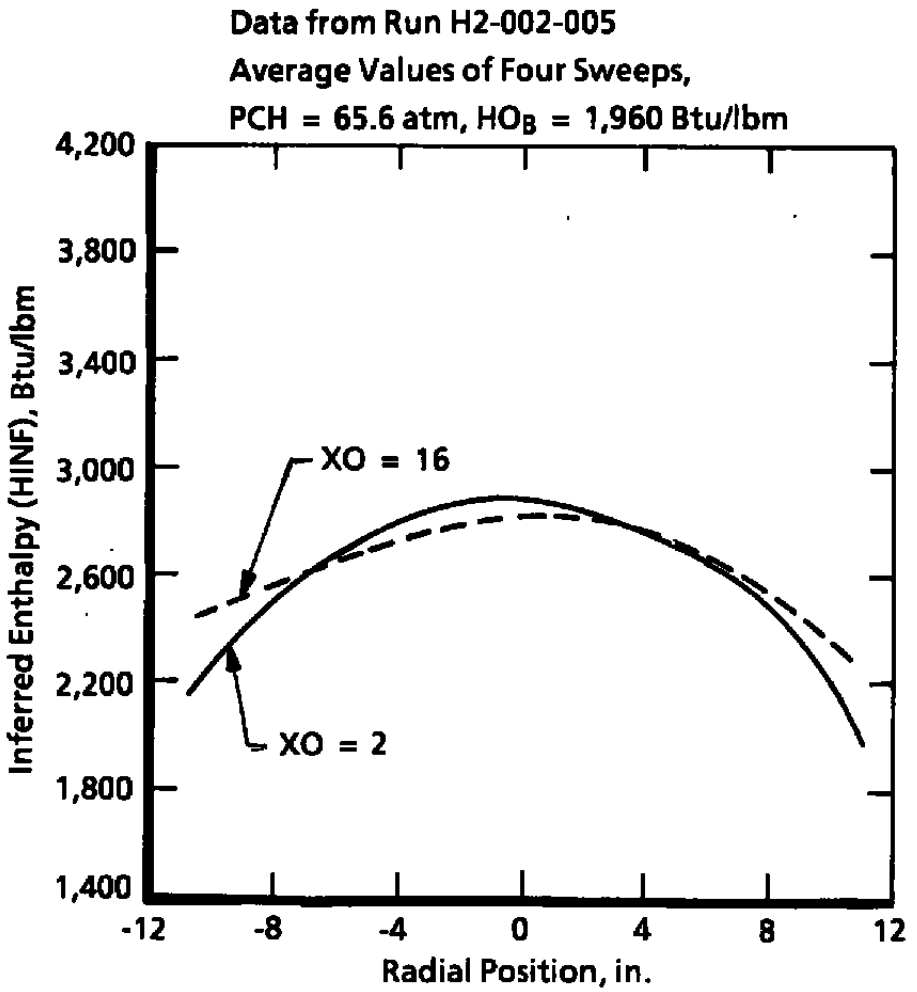

Figure 24. Inferred enthalpy comparisons of data from two axial stations.

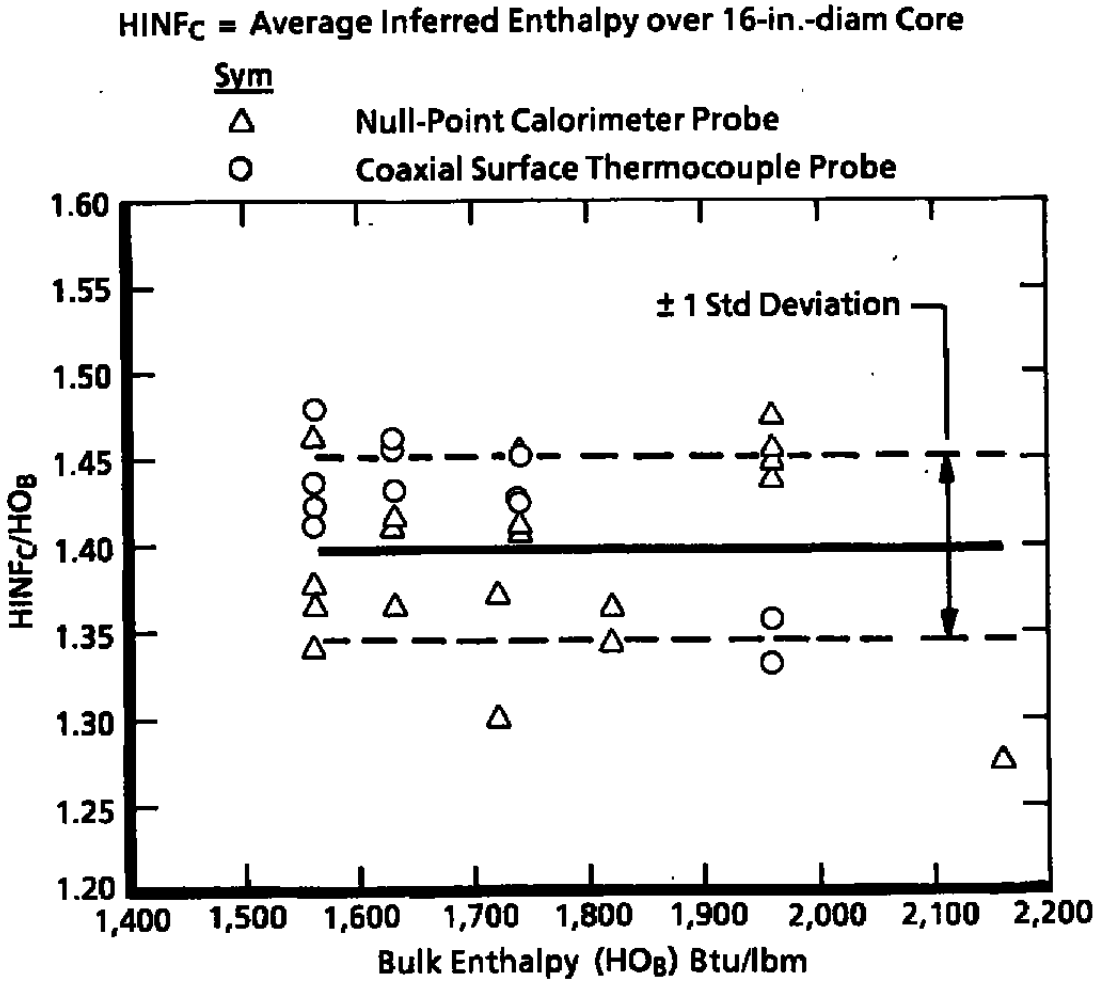

Figure 25. Average enthalpy in the free-jet 16-in.-diam core versus the heater bulk enthalpy.

Table 1. Test Matrix

$D^* = 1.5$ in., $D_E = 24$ in., Flat Enthalpy Profile

HEAT-H2 Run No.	Axial Station (XO), in.	Transformer Tap Setting No.	Air Mass Flow, lbm/sec	Arc Current, amps	Arc Voltage, kv	Arc Chamber Pressure, atm	Bulk Enthalpy, Btu/lbm	Probe/Model Sweep No.						Sweep Direction
								Standard Calorimeter	Standard Pitot	Coax	Flow Angle	Water-Cooled Pitot	Blunt Cone	
002-001	2	16	5.7	2,070	9.36	37	1,820	2	1	—	101	102	103	CCW
002-001	2	16	5.7	2,070	9.36	37	1,820	4	3	---	106	105	104	CW
002-001	9	16	5.7	2,070	9.36	37	1,820	6	5	—	107	108	109	CCW
002-001	16	16	5.7	2,070	9.36	37	1,820	8	7	—	112	111	110	CW
002-001	16	16	6.6	1,980	10.49	42.2	1,720	10	9	---	113	114	115	CCW
002-001	2	16	6.6	1,980	10.49	42.2	1,720	12	11	—	118	117	116	CW
002-001	2	25	5.2	2,800	8.25	36.6	2,160	14	13	—	119	120	121	CCW
002-002	16	25	5.2	2,830	8.3	37.5	2,000	2	1	—	101	102	103	CCW
002-002	2	25	5.2	2,830	8.3	37.5	2,000	4	3	---	106	105	104	CW
002-002	2	27	7.6	2,850	11.00	52	1,910	6	5	—	107	108	109	CCW
002-002	16	27	7.6	2,850	11.00	52	1,910	8	7	---	112	111	110	CW
002-002	2	27	7.6	2,850	11.00	52	1,910	10	9	---	113	114	115	CCW
002-005	2	29	9.8	2,900	12.5	65.6	1,960	1	—	2	101	102	103	CCW
002-005	2	29	9.8	2,900	12.5	65.6	1,960	7	—	8	106	105	104	CW
002-005	16	29	9.8	2,900	12.5	65.6	1,960	9	—	10	107	108	109	CCW
002-005	16	29	9.8	2,900	12.5	65.6	1,960	15	---	16	112	111	110	CW
002-005	16	27	7.6	2,810	10.5	51.4	1,980	17	—	18	113	114	115	CCW
002-006	2	14	5.2	1,820	8.9	32	1,630	1	—	2	101	102	103	CCW
002-006	9	14	5.2	1,820	8.9	32	1,630	7	---	8	106	105	104	CW
002-006	16	14	5.2	1,820	8.9	32	1,630	9	---	10	107	108	109	CCW
002-006	16	17	9.2	1,940	13.2	55	1,560	15	—	16	112	111	110	CW
002-006	9	17	9.2	1,940	13.2	55	1,560	17	—	18	113	114	115	CCW
002-006	2	17	9.2	1,940	13.2	55	1,560	23	---	24	118	117	116	CW
002-006	2	17	9.2	1,940	13.2	55	1,560	25	---	26	119	120	121	CCW
002-006	2	20	9.2	2,315	12.7	58	1,740	31	—	32	124	123	122	CW
002-006	16	20	9.2	2,315	12.7	58	1,740	33	---	34	125	126	127	CCW
002-006	9	20	9.2	2,315	12.7	58	1,740	39	---	40	130	129	128	CW

CCW = Counterclockwise
CW = Clockwise

Table 2. Model Positioner System Sweep Sequences

Counterclockwise* Sweep Sequence

Run H2-002-001

Probe†	Total Sweep Angle, deg	Sweep Rate, deg/sec	Pause on Centerline**
Standard Pitot & Calorimeter	72	60	No
Flow Angle	72	6	Yes
W-C Pitot	72	12	Yes
Blunt Cone	72	60	Yes

Runs H2-002-002 – H2-002-006

Probe†	Total Sweep Angle, deg	Sweep Rate, deg/sec	Pause On Centerline**
Standard††	72	60	No
Flow Angle	72	6	No
W-C Pitot	72	30	Yes
Blunt Cone	72	60	Yes

Clockwise* Sweep Sequence

Run H2-002-001

Probe†	Total Sweep Angle, deg	Sweep Rate, deg/sec	Pause on Centerline**
Blunt Cone	72	60	Yes
W-C Pitot	72	12	Yes
Flow Angle	72	6	Yes
Standard Cal. & Pitot	72	60	No

Runs H2-002-002 – H2-002-006

Probe†	Total Sweep Angle, deg	Sweep Rate, deg/sec	Pause On Centerline**
Blunt Cone	72	60	Yes
W-C Pitot	72	30	Yes
Flow Angle	72	6	No
Standard††	72	60	No

* Direction when viewed looking downstream.
† Indicates order probes pass through flow field.
** Nominally, 0.5-sec pause by dividing sweep into two 36-deg sweeps.
†† For Runs H2-002-005 and H2-002-006, the standard pitot probe was replaced by a coaxial surface thermocouple probe.

APPENDIX A
Flow Angle Probe Data Reduction

PAVG = Average probe pressure
= (PFA1P + PFA2P + PFA3P + PFA4P)/4, psia

where PFA1P ... PFA4P are the probe pressures, psia

$\frac{PAVG}{PPWCP}$ = ratio of average probe pressures to the corresponding pitot pressure, nondimensional

DP13 = PFA1P − PFA3P, psia

DP24 = PFA2P − PFA4P, psia

$$DPSQ = \sqrt{\left(\frac{DP13}{PAVG}\right)^2 + \left(\frac{DP24}{PAVG}\right)^2}, \text{ nondimensional}$$

MLC = local Mach number, defined as function of (PAVG/PPWCP, DPSQ):

$$MLC = \sum_{i=0}^{3} a_i(PAVZPP)$$

a_i = function of PAVZPP (segmented curve fit)

PAVZPP	a_0	a_1	a_2	a_3
< 0.228	633.243	−8630.68	39684.3	−61117.2
≥ 0.228; < 0.455	18.36484	−112.933	267.146	−218.733
≥ 0.455; < 1	3.11927	−3.11927	0	0
≥ 1; ≤ 0	0	0	0	0

PAVZPP = measured value of PAVG/PPPWCP adjusted to what would be obtained at zero angle of attack.

$= (PAVG/PPWCP)/(1 + b_1(DPSQ) + b_2(DPSQ)^2)$

$b_1 = -0.002666$

$b_2 = 0.01636$

AATCA = total pitch angle sensed by the flow angularity probe, relative to the probe axis, computed from curve fit, deg

$$AATCA = GCOR \cdot MCOR \cdot [a_1(DPSQ) + a_2(DPSQ)^2]$$

where

GCOR = correction for γ other than $\gamma = 1.4$

MCOR = correction for Mach number other than MLC = 6.

- $GCOR = 1 + \frac{(1.4 - \gamma)}{0.2}(GRAT - 1)$

$$GRAT = C_1 + C_2(MLC) + C_3(MLC)^2$$

$C_1 = 1.10443$
$C_2 = -0.02424$
$C_3 = 0.00141$
MLC ~ previously defined
$\gamma = 1.3$, assumed

- $MCOR = b_1 + b_2(MLC) + b_3(MLC)^2$

$b_1 = 1.97169$
$b_2 = -0.25954$
$b_3 = 0.01622$

- DPSQ ~ previously defined

$a_1 = 7.24165$
$a_2 = 0.38162$

APPENDIX B
HEAT-HR Performance Correlation Equations

$$\text{Air Mass Flow (lbm/sec)} = WA = \frac{1.4603 \cdot DSTAR^2 \cdot PCH}{HO_B^{0.4002}}$$

$$\text{Arc Heater Chamber Pressure (atm)} = PCH = \frac{4.0336 \cdot I^{0.1664} \cdot WA}{DSTAR^2}$$

$$\text{Voltage (kv)} = V = \frac{3.253 \cdot WA^{0.7}}{DSTAR^{0.3883}}$$

where

HO_B = Bulk enthalpy, Btu/lbm

I = Arc current, amp

DSTAR = Nozzle throat diameter, in.

NOMENCLATURE

A^*	Area of nozzle throat, in.^{2}
AATCA	Total flow angle with respect to probe (see Fig. 12a), deg
A_{GEO}	Geometric area of free jet, in.^{2}
ALPHA	Flow divergence from nozzle centerline (see Fig. 12b), deg
Cp	Specific heat at constant pressure, Btu/lbm-°F
CCW	Counterclockwise looking downstream
COAX	Coaxial surface thermocouple
CW	Clockwise looking downstream
D^*, DSTAR	Nozzle throat diameter, in.
D_E	Exit diameter of nozzle, in.
DALPHA	Flow divergence from conical theory, deg
DPSQ	Square root of the sum of the squares of the differential static pressure measurements divided by the average static pressure measurement of the flow angle probe (see Appendix A)
γ, GAMMA	Ratio of specific heats
HINF	Total enthalpy inferred from measurements of heat flux and pitot pressure, Btu/lbm
$HINF_c$	Average of HINF within a 16-in.-diam core of the free jet, Btu/lbm
HO_B	Total enthalpy of the air as it leaves the nozzle as defined by an energy balance, Btu/lbm
H_v	Enthalpy of air at metering venturi, Btu/lbm

K	Thermal conductivity, Btu/sec-ft-°F
M	Mach number
MLC	Local Mach number computed from probe measurement, used for flow angle coefficient definition
NO	Nitric oxide
NO_2	Nitrogen dioxide
NO_x	Sum of constituents of nitric oxide and nitrogen dioxide, percent
P	Pressure on surface of blunt cone, psia
PAVG	Average static pressure of flow angle probe, psia
Pnose	Blunt cone stagnation pressure, psia
PCH	Arc heater chamber pressure, atm or psi
PHI	Roll orientation of the flow vector with respect to the probe axis (see Fig. 12a), deg
PPWCP	Water-cooled pitot pressure probe measurement, psia
PROFILE	Heater enthalpy profile shape, either flat or peaked
PSI	Flow angle in the circumferential direction (see Fig. 12b), deg
$\dot{q}$	Heat flux, Btu/ft^2-sec
R	Radius, in.
R*	Radial distance from source flow to the sonic point (nozzle throat), in.
RADIAL POSITION	Radial position of probe relative to nozzle centerline (positive above centerline), in.

R_E	Radius of nozzle exit, in.
ϱ	Material density, lbm/ft^3
ϕ	Circumferential location of orifices on blunt cone (0 deg on top, positive clockwise looking downstream), deg
STD CAL	Standard null-point calorimeter probe
STD PITOT	Standard pitot pressure probe
SWEEP	Sequence number of data sets within a RUN (see Table 1)
T	Temperature, °R
t	Time, sec
UP,VP,WP	Velocity vector components with respect to the flow angle probe (see Fig. 11a), ft/sec
UF,VF,WF	Velocity vector components with respect to the tunnel (see Fig. 11b), ft/sec
VL	Total local velocity, ft/sec
WA	Mass flow of air, lbm/sec
W-C PITOT	Water-cooled pitot pressure probe
X	Distance along blunt cone body centerline, in.
XO	Distance along nozzle centerline from nozzle exit plane, in.
XP,YP, ZP	Flow angle probe coordinates (see Fig. 11a), in.